5-2018

Experimental and Computational Studies of Rotation and Proton Tunneling in Organic Molecules and Molecular Dimers

Agapito Serrato III
The University of Texas Rio Grande Valley

Recommended Citation

Serrato, Agapito III, "Experimental and Computational Studies of Rotation and Proton Tunneling in Organic Molecules and Molecular Dimers" (2018). *Theses and Dissertations*. 173.
https://scholarworks.utrgv.edu/etd/173

EXPERIMENTAL AND COMPUTATIONAL STUDIES OF ROTATION AND PROTON TUNNELING IN ORGANIC MOLECULES AND MOLECULAR DIMERS

A Thesis

by

AGAPITO SERRATO III

Submitted to the Graduate College of
The University of Texas Rio Grande Valley
In partial fulfillment of the requirements for the degree of

MASTER OF SCIENCE

May 2018

Major Subject: Chemistry

EXPERIMENTAL AND COMPUTATIONAL STUDIES OF ROTATION AND PROTON TUNNELLING IN ORGANIC MOLECULES AND MOLECULAR DIMERS

A Thesis
by
AGAPITO SERRATO III

COMMITTEE MEMBERS

Dr. Wei Lin
Co-Chair of Committee

Dr. Shervin Fatehi
Co-Chair of Committee

Dr. Celia Flores-Feist
Committee Member

Dr. Arnulfo Mar
Committee Member

Dr. Evangelia Korikotsu
Committee Member

May 2018

ABSTRACT

Serrato III, Agapito, Experimental And Computational Studies of Rotation And Proton Tunneling In Organic Molecules And Dimers. Master of Science (MS), May, 2018, 83 pp., 12 tables, 24 figures, references, 128 titles.

An introduction to the relations of classical and quantum mechanics are presented in brief. As is an overview of the instrumentation and quantum chemical analysis performed to characterize the molecules presented in in this thesis. The pure rotational spectrum of 3,3,3-trifluoro-2(trifluoromethyl)propanoic acid, perfluorobutyric acid–formic acid dimer, and tropolone–formic acid dimer were measured using high-resolution microwave spectroscopy. The spectra have been observed using a cavity-based Fourier-transform microwave (FTMW) spectrometer and/or a chirped-pulse FTMW

DEDICATION

To my loving parents Agapito and Juanita and my sisters Joanna and Sarah Isabel Serrato. Thank you for always supporting me as I strived to do my best. To my loving Wife, Nina, thank you and I Love you.

ACKNOWLEDGEMENTS

There are too many people to mention by name. But I will do my best to mention as many as I can. I would like to thank several people who have provided me with unwavering support and guidance over the years. First and foremost, I would like to thank my Mother and Father without whose love, support, and sacrifices I never would have been afforded opportunity to pursue my dreams. There were too many occasions that were sacrificed for this journey to come to fruition. It would have been infinitely harder to accomplish this milestone without all of you and your support.

Thank you to all of my teachers and professors over the years. I’ve had the fortune and opportunity to learn from very passionate and knowledgeable people. Your friendship, patience, and instruction have been and always will be welcome. I would specifically like to thank Mr. Frank Gonzalez inspired me in your chemistry class at San Benito High School and of course to both Dr. Wei Lin and Dr. Shervin Fatehi. Without either of you I’d never have gotten this far. Dr. Lin, you’ve always had my studies as the primary goal of our collaboration over the years. You gave me an opportunity many years ago to work with you, and that has allowed me to continuously improve myself by expanding my horizons not only as a student, but as a researcher and as an individual. You are an integral part of my continued success, and I do not doubt that without your support over the years I would not be here writing this textDr. Fatehi, you have helped me bridge a knowledge gap. A gap sometimes seemed like a chasm of unknowable depth

and breadth. It’s the first step that always seems to be the hardest, and your guidance helped me round out my knowledge and most definitely improve my skillset. Both of you inspire me daily and I hope to carry forth and represent your teachings well. My thanks go out to all of the members past and present to the Lin group: Michael Carrillo, Alex Treviño, Tania Veronica Alvarez Castro and the Fatehi group members: Daniel Piñon, Catherine Clark, and Jorge Garcia.

I’d also like to thank all of our collaborators: Dr. Wolfgang Jäeger, and Dr.Yunjie Xu at the University of Alberta , Dr. Stephen G Kukolich and Mr. Aaron M. Pejlovas at the University of Arizona for their hospitality, and Dr. G. Schmitty Grubbs (GSG), Dr. Daniel A. Obenchain (DAO), Dr. Stewart E. Novick at Wesleyan University, and Dr. Steven A. Cooke (SAC) at Purchase College (SUNY Purchase), formerly of University of North Texas. Currently, G.S.G. is at the University of Missouri Science and Technology as an Assistant Professor of Chemistry, D.A.O. is at Leibniz Universität Hannover as an Alexander von Humboldt Research Fellow

I’d like to thank University of Texas Rio Grande Valley (UTRGV) Graduate Office and the Welch Foundation for financial support to attend the 253rd American Chemical Society.

“*When Chekhov saw the long winter, he saw a winter bleak and dark and bereft of hope. Yet we know that winter is just another step in the cycle of life. But standing here among the people of Punxsutawney and basking in the warmth of their hearths and hearts, I couldn't imagine a better fate than a long and lustrous winter.* “

– Phil Connors, Groundhog Day

TABLE OF CONTENTS

LIST OF TABLES

Page

LIST OF FIGURES

CHAPTER I

INTRODUCTION

Uncertainty may cause anxiety in many people. But if you are making observations on an atomic level, not knowing exactly how an electron behaves under certain conditions is the core of the Heisenberg uncertainty principle.[1] But we can’t just start with Heisenberg. The very concept of the atomic model has undergone several refinements over the last century. The contribution by the world scientific communities cannot be overstated. The evolution of the atomic model beginning with Democritus, advancing to Dalton’s model, and to the currently accepted quantum mechanical theory have spurred new fields of interest to be opened for investigation. The previous combined works of those who came before us allows the works in this thesis to be described by the authors.

When we first decide on a system to analyze we have to try and describe it. Ideally, we would like to model a system exactly. Unfortunately, that is usually not possible with most systems that we investigate and so the models we use tend to be defined in terms of what’s feasible. If we were to anthropomorphize atoms and molecules we could say that they “walk around.” We know that molecules don’t “walk” but they do move in three-dimensional space and the motions of these particles are described by well-known motions such as: rotational, vibrational, and translational motion(s). The simplest model that can describe all of these features is the diatomic model which allows us to describe the rotations of the system rotational motions can be evaluated using Microwave spectroscopy. The quantum chemical (QM) package Gaussian [2] can be used to assist in the assignment of the spectra for the molecule(s) of interest. The systems we are currently interested in are either monomer or dimer systems. We were able to use the High Performance Computing (HPC) Lonestar cluster at the Texas Advanced Computing Center which is located on The University of Texas at Austin campus. This facility allowed us to calculate systems quicker than we had been previously capable of. The results of the QM calculations could be utilized in programs like Herb Pickett's SPCAT/SPFIT suite [3] and the PGOPHER program from Dr. Colin Western's group at the University of Bristol to calculate a simulated spectrum to compare to the experimental spectra. [4,5]

The impetus for the investigation of the molecules in this thesis started with an article in Chemical & Engineering News regarding the phasing out of the production of a feed component, perfluorooctanoic acid, which is the telomer of a ubiquitous item of modern life, Teflon. The article details the recommnedations of The United States Environmental Protection Agency (USEPA) which has worked with the the manufacturers who voluntarily agreed to phase out the production of perfluorooctanioc acid (PFOA) in the United States at the end of 2015. This piqued our interest in PFOA as it's one of the oligomers for Teflon. Because perfluorinated carboxylic acids interaction with the environment and its robust stability when solvated most PFCAs are considered persistent organic pollutants. With our interest peaked we set out to characterize and ultimately discuss the interaction between these systems and the environment by investigating the monomer and then systematically building up the first solvation shell of these perfluorinated carboxylic acids (PFCAs). The interaction is important due to the increasing concern that the perfluoro-monomers of perfluorooctanoic acid have been linked to an increase in cancer rates in surrounding areas near the production sites and as mentioned a production ban was implemented by the USEPA. [6]

The first molecule named perfluorobutyric acid has been investigated by our group previously [7] and the perfluorobutyric acid – formic acid system presented in this thesis continues an ongoing investigation of these molecules by us and our collaborators. Perfluorinated carboxylic acids are a special class of compounds with considerable industrial applications. In this study, we applied high-level ab initio calculations together with chirped pulse and cavity-based Fourier transform microwave spectroscopy to investigate the structural and possible tunneling properties of the Perfluorobutyric Acid—Formic Acid complex. Only one clearly dominant conformer, featuring an eight-membered double hydrogen-bonded pseudo-ring, was predicted for the hetero acid dimer and detected experimentally. The rotational constants calculated at the B3LYP-D3BJ/6-311++G (2d, p) level are in excellent agreement with the experimental ones. No tunneling splittings were detected in the experimental spectra. Detailed analyses of the non-covalent intermolecular interactions in the hetero acid dimer provide an explanation for the absence of double proton transfer and identify the presence of F—F attractive interactions.

The microwave spectrum was measured for the doubly hydrogen-bonded dimer formed between tropolone and formic acid. The predicted symmetry of this dimer was C_{2v}(M), and it was expected that the concerted proton tunneling motion would be observed. After measuring 25 a- and b-type rotational transitions, no splittings which could be associated with a concerted double proton tunneling motion were observed. The calculated barrier to the proton tunneling motion is near 15 000 cm^{-1}, which would likely make the tunneling frequencies too small to observe in the microwave spectra. The rotational and centrifugal distortion constants determined from the measured transitions were A = 2180.7186(98) MHz, B = 470.873 90(25) MHz, C = 387.689 84(22) MHz, D_J = 0.0100(14) kHz, D_{JK} = 0.102(28) kHz, and D_K = 13.2(81) kHz. The B3LYP/aug-cc-pVTZ calculated rotational constants were within 1% of the experimentally determined values.

There exist a few different techniques that could be used to analyze molecules in Microwave spectroscopy. As it is a bit of a niche technique there are only 52 groups around the world with over 1000 active projects. While many may not be entirely familiar with Fourier Transform MW spectroscopy, the standard instrument most chemists learn about in their undergraduate careers is Fourier transform nuclear magnetic resonance (FT-NMR) and there are parallels which of course include the Fourier transform of time domain signal into the frequency domain. [8] The difference between MW spectroscopy and other common spectroscopic techniques is due to the nature of what's being explored. For instance, in the case of Ultraviolet/Visible spectrometer the wavelengths used will excite the electrons in a molecule. But, in the case of an infrared spectrometer the use of IR energy excites the vibrational "springs" between atoms. While MW, on the other hand, excites the entire molecule and induces an increase in molecular rotational frequency.[9]

Thesis Outline

This thesis presents and characterizes the rotational spectra of several Poly- and Perfluorinated Carboxylic Acid—Formic Acid dimers.

Chapter 2 outlines the theory of rotational spectroscopy and the reason we can use the time-independent Schrödinger equation for dynamical systems. The computational methods used to explore the quantum chemical landscapes that these molecules inhabit.

Chapter 3 introduces the uses and application of the concepts that were presented in Chapter 2. Here we introduce the various types Fourier transform microwave spectrometers that were used in the research and the differences between them.

Chapter 4 describes the interaction of perflurobutyric acid-formic acid dimer (PFBA-FA) through computational analysis of the potential energy surface to investigate the double proton tunneling action in this system using both a cavity and chirped pulse Fourier transform microwave spectrometer.

Chapter 5 we report a combined MW spectroscopic and ab initio study of a representative branched polyfluorinated carboxylic acid, 3,3,3-trifluoro-2-(trifluoromethyl)propanoic acid (TTPA). The MW experiments were carried out at the University of Alberta using both chirped-pulse and cavity-based Fourier-transform MW (FTMW) spectrometers. The experimental work was complemented by high-level quantum chemistry calculations, from which multiple low-energy conformers were located. Using this approach, we identified the most stable conformers of TTPA experimentally.

Chapter 6 This work was performed at the University of Arizona in Dr. Stephen Kukolich’ lab. Tropolone (2-hydroxy-2,4,6-cycloheptatrien-1-one), is a seven-membered pseudoaromatic molecule and is considered as a prototypical molecule for intramolecular proton transfer. Formic acid (FA) is known to form doubly hydrogen-bonded dimers with several carboxylic acids [10–16] that exhibit a concerted double proton tunneling. Some other doubly hydrogen-bonded dimers do not exhibit the concerted proton tunneling. [17,18] The microwave spectrum of cyclopropanecarboxylic acid—formic acid (CPCA—FA) dimer [19] was reported and no tunneling was observed for this doubly hydrogen-bonded dimer. The doubly hydrogen-bonded tropolone–formic acid dimer introduces a new interesting question about whether or not the tunneling splitting can be observed in this larger more symmetric complex.

CHAPTER II

THEORY OF MOLECULAR ROTATION

Angular momentum and moments of inertia

The classical theories used to describe the motions of larger bodies cannot be used to describe systems on the microscopic scale like atoms and molecules, let alone subatomic particles. We can connect these concepts with the correspondence principle. \Which states that the system can be described by the theory of quantum mechanics or by quantum theory which reproduces chemical physics in the limit of large quantum numbers.[20,21] So, for large orbits and for large energies quantum calculations must agree with classical calculations.[22] This theory is integral to our ability to try and impose known macroscopic concepts onto microscopic small system.

Consider an object moving in a plane at a constant speed and at a constant distant from a fixed point.

We can translate the concept of linear momentum, p, which is the product of the mass and velocity of the particle.

$$p = mv \tag{1}$$

We can recast the velocity, v, of the system in order to emphasize the rotation around the ring. This rotational frequency, v_{rot} is now considered with the distance, r, from the center of rotation and thus the object is rotating around the circumference of a circle. We know circumference, $C = 2\pi r$, and we can rewrite linear velocity as angular velocity, $v = 2\pi v_{rot} = r\omega_{rot}$ which has units of radians per second. Since we will be interested in the kinetic energy, T, of a particle revolving around a fixed point. is described by the following equations

$$K = \tfrac{1}{2}mv^2 = \tfrac{1}{2}mr^2\omega^2 = \tfrac{1}{2}I\omega^2 \tag{2}$$

The moment of inertia, I, is equal to mr^2 and we can see that there is a correspondence between the variables $\omega \leftrightarrow v$ and $I \leftrightarrow m$. This correlation is further elaborated, Figure 2, which illustrates a fundamental quantity in a rotating system. Angular momentum is defined as the cross product of the momentum and the radius.

$$\vec{L} = \vec{p} \times \vec{r} = mvr = (mr^2)\left(\frac{v}{r}\right) = I\omega \tag{3}$$

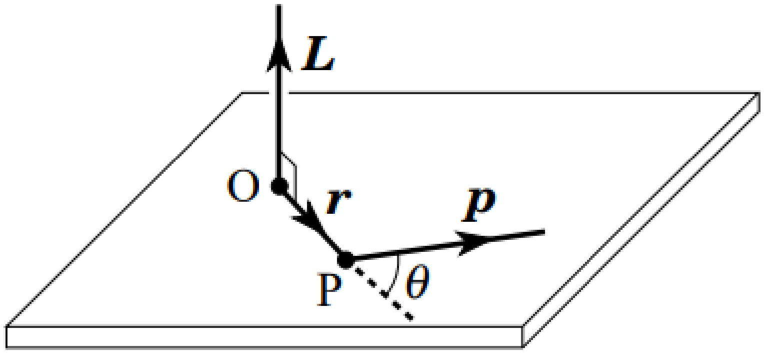

Figure 1: Angular momentum, $\vec{L}$, of a particle P about a point O. [23]

This simple model is generalized from a single particle rotating around a fixed point, to a system with two particles that can be of different masses. As in the case of the ionic heteronuclear compound hydrogen fluoride, HF. In the general form, the center of mass of this system is also the center of rotation, and the two particles rotate about this fixed point. This simple model is the rigid rotor.

Types of Motion	
Linear	Angular
Mass (m)	Moment of Inertia (I)
Speed (v)	Angular speed (ω)
Momentum (p = mv)	Angular momentum ($\hat{l} = I\omega$)
Kinetic Energy $\left(K = \frac{mv^2}{2} = \frac{p^2}{2m}\right)$	Rotational Kinetic Energy $\left(K = \frac{I\omega^2}{2} = \frac{l^2}{2I}\right)$

Table 1 The correspondences between linear systems and rotating systems. Adapted from McQuarrie's Quantum Chemistry. [1]

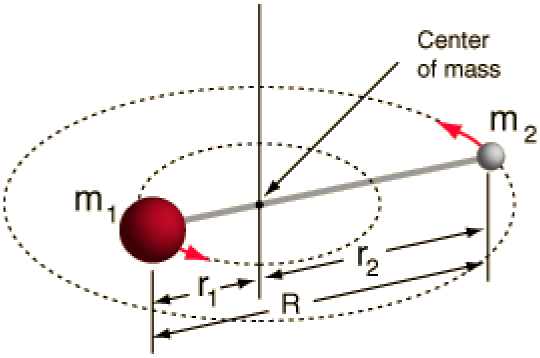

Figure 2: Two masses rotating about their center of mass.[24]

The center of mass, in Figure 3, for this system of two particles is a point on the line connecting the two centers and is described by the following equation:

$$m_1 r_1 = m_2 r_2 \tag{4}$$

Where $R \equiv r_1 + r_2$ is the distance from the center of each rotating mass to the center of rotation and the distance between the two objects is the sum of the two distances. It should be noted that with a fixed distance, R, that mass m_1 must rotate slower than m_2 because $C_1 < C_2$ but $\tau_1 = \tau_2 \equiv \tau$.

Using algebra to rearrange and isolate r_1 and r_2 from the previous equations (4) & the relation $R \equiv r_1 + r_2$ give us

$$r_1 = \frac{m_2}{m_1 + m_2} R \qquad r_2 = \frac{m_1}{m_1 + m_2} R \tag{5}$$

And if we look at (2) we can include the two different particles into the original equations.

$$T = \tfrac{1}{2} m_1 v_1^2 + \tfrac{1}{2} m_2 v_2^2 \tag{6}$$

As previously mentioned that through substitution $v = \omega r$ and we can make a similar substitution in (6).

$$\begin{aligned} T &= \tfrac{1}{2} m_1 r_1^2 \omega^2 + \tfrac{1}{2} m_2 r_2^2 \omega^2 \\ &= \tfrac{1}{2}(m_1 r_1^2 + m_2 r_2^2)\omega^2 \\ &= \tfrac{1}{2} I \omega^2 \end{aligned} \tag{7}$$

This simplification leads us to a representative quantity known as the moment of inertia of the system. The form for the general case:

$$I = \sum_{i=1}^{n} m_i \left|\bar{r}_i\right|^2 \tag{8}$$

And the for the linear molecule

$$I = \left(\frac{m_1 m_2}{m_1 + m_2} \right) R^2 \tag{9}$$

We may identify the quantity in parentheses as the reduced mass.

$$\mu = \frac{m_1 m_2}{m_1 + m_2} \tag{10}$$

Substituting (10) into (8) we can now write

$$I = \mu R^2 \tag{11}$$

This concept has two limiting cases. The first when $m_1 = m_2 \equiv m \Rightarrow \mu = (m/2)$ and the other is when $m_1 \gg m_2 \Rightarrow \mu = m_2$. The concept of reduced mass (10) and the moment of inertia (11) will be revisited when begin talking about rotational constants and how they apply in general to decoding the spectra of various molecules.

Now that we have started to build a foundation we can begin to make several relations regarding the kinetic energy of a particle or particles as they(13) rotate on a ring.

The kinetic energy of a particle rotating on a ring can be described as follows.

$$K = \frac{1}{2}\mu v^2 = \frac{1}{2}\mu r^2\omega^2 = \frac{1}{2}I\omega^2 \tag{12}$$

$$\vec{L} = pr\sin\theta = \mu vr\sin\theta \tag{13}$$

$$p = \frac{l}{r} \quad \text{when } \theta = \frac{\pi}{2} \tag{14}$$

Using equations (13) and (14) with an equivalent expression for the kinetic energy, we confirm the expression given in Table 1.

$$K = \frac{p^2}{2\mu} = \frac{l^2}{2\mu r^2} = \frac{l^2}{2I} \tag{15}$$

Bridging the gap: 2D quantum mechanics

$$\hat{H} = \frac{\hat{p}^2}{2\mu} = -\frac{\hbar^2}{2\mu}\left(\frac{\partial^2}{\partial x^2} + \frac{\partial^2}{\partial y^2}\right) \tag{16}$$

Acting on a wave function Ψ

$$\hat{H}\Psi = E\Psi \tag{17}$$

$$-\frac{\hbar^2}{2\mu}\left(\frac{\partial^2\Psi(x,y)}{\partial x^2} + \frac{\partial^2\Psi(x,y)}{\partial y^2}\right)\Bigg|_{r=r_o} = E\Psi(x,y) \tag{18}$$

Then we can change the coordinates from x and y to r and ϕ .

$$\Psi(x, y) = \Psi(\phi, \theta) \tag{19}$$

$$-\frac{\hbar^2}{2\mu r^2}\frac{\Phi(\phi)}{d\phi^2} = E\Phi(\phi) \tag{20}$$

Where $\Phi(\phi)$ is the rotational eigenfunction.

$$\Phi(\phi) = \Phi(\phi + 2\pi) \tag{21}$$

$$\Phi \pm (\phi) = A_{\pm\phi} e^{i|m_l|\phi} \tag{22}$$

$$\begin{aligned} e^{im_l\phi} = e^{im_l(\phi+2\pi)} &= e^{im_l\phi}e^{im_l 2\pi} \\ &= \cos(2\pi m_l) + i\sin(2\pi m_l) = 1 \\ &= \cos(2\pi m_l) = 1 \;\; ; \;\; m_l = 0, \pm 1, \pm 2, \pm 3, ... \end{aligned} \tag{23}$$

One boundary condition leads to one quantum number m_l .

The normalization of the wave function is essential.

Given that m_l is an integer, ω will take finite values and will have a discrete set of rotational frequencies.

The energy, E, from equation (20) can be described by the following equation.

$$E_{m_l} = \frac{\hbar^2 m_l^2}{2\mu r_o^2} = \frac{\left|\hat{l}^2\right|}{2\mu r_o^2} = \frac{\left|\hat{l}^2\right|}{2I} = \frac{1}{2}I\omega^2 \tag{24}$$

The wavefunction of a rigid rotor is the same as the wavefunction of a free particle restricted to a circle (particle on a ring) are the same after removing the rotational motion on the ring.

$$E_{kinetic} = \frac{1}{2}\mu v^2 = \frac{1}{2}\mu r^2\omega^2 \tag{25}$$

For a rigid rotor, the angular momentum lies in the z-direction, if rotating in the xy plane, and l_z is the angular momentum operator. Due to the definition of the rigid rotor model which is a linear diatomic molecule the rotation between two axes

$$\hat{l}_z = -i\hbar \frac{\partial}{\partial \phi} \tag{26}$$

For the l_z operator is the angular analogue of momentum. This is expressed in equation (23), and the quantization of angular momentum rises. Because of the uncertainty principle the position, ϕ, cannot be measured precisely the probability for any interval of $d\theta$ is the same.

Transformation of Cartesian to Spherical Coordinates

To move from a 2D rigid rotor to a 3D rigid rotor. We must have some method to describe the increased number of parameters easily. We will do this with the transformation of the Cartesian plane system to the more convenient spherical coordinate system. Recall that the relationships for the 2D polar system are as follows. A plane polar coordinate system uses the variables (r,φ) as shown in the diagram below, to describe the position of points, curves, and areas.

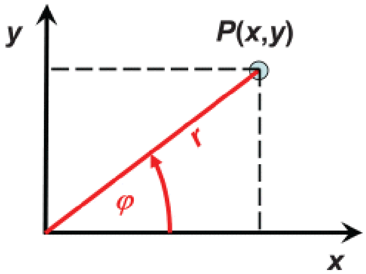

Figure 3: In Cartesian coordinates, the position of point P is given by its (x,y)-coordinates. Polar coordinates use the distance r from the origin and the angle φ from the x-axis (shown in red color); the point is then described by P(r,φ). Taken in entirety from [25].

Conversion from Cartesian to polar coordinates can be accomplished by the following substitutions:

$$\begin{aligned} x &= r\cos\varphi \qquad & y &= r\sin\varphi \\ r &= \sqrt{x^2+y^2} \qquad & \varphi &= \tan^{-1}\left(\frac{y}{r}\right) \end{aligned} \tag{27}$$

In addition to the x and y-axis, the 3D Cartesian system uses a z-axis orientated in a right-hand system as shown below in Figure 5.

The polar coordinates are:

1. The distance r from the origin.
2. The angle θ from the z-axis (zenith angle).
3. The angle of φ from the x-axis (azimuth angle).

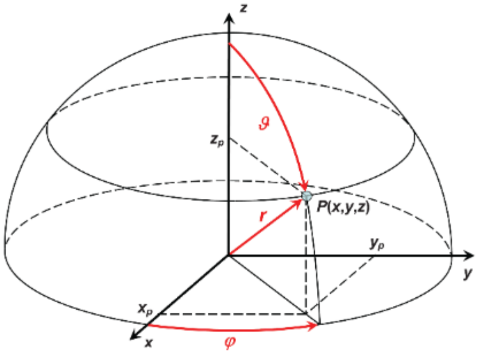

Figure 4: In Cartesian coordinates, the position of point P is given by its (x_p,y_p,z_p) coordinate values (where index p serves to distinguish coordinate values of P and the coordinate axes). Polar coordinates use (shown in red) the distance r and the angles φ and ϑ; the point is then represented by $P(r_p,\vartheta_p,\varphi_p)$.[25]

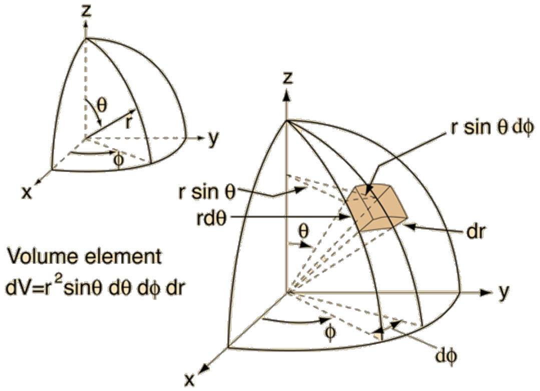

Figure 5: Additional presentation of the spherical coordinate system. [26]

Conversion from Cartesian to polar coordinates are as follows:

$$x = r\sin\theta\cos\phi \qquad y = r\sin\theta\sin\phi \qquad z = r\cos\phi$$
$$r = \sqrt{x^2+y^2+z^2} \qquad \phi = \tan^{-1}\left(\frac{y}{r}\right) \quad \theta = \tan^{-1}\left(\frac{\sqrt{x^2+y^2}}{z}\right) \tag{28}$$

So, after the transformation process, we obtain the following.

$$\begin{aligned}
\hat{\mathbf{L}}_x &= -i\hbar(-\sin\phi\frac{\partial}{\partial\theta} - \cot\theta\cos\phi\frac{\partial}{\partial\phi}) \\
\hat{\mathbf{L}}_y &= -i\hbar(-\cos\phi\frac{\partial}{\partial\theta} - \cot\theta\sin\phi\frac{\partial}{\partial\phi}) \\
\hat{\mathbf{L}}_z &= -i\hbar\frac{\partial}{\partial\phi}
\end{aligned} \tag{29}$$

This transformation and a little extra work allow us to express the Laplacian in spherical coordinates.

$$\begin{aligned}
\nabla^2 &= \frac{1}{r^2}\frac{\partial}{\partial r}\left(r^2\frac{\partial}{\partial r}\right)_{\theta,\phi} + \frac{1}{r^2\sin\theta}\frac{\partial}{\partial\theta}\left(\sin\theta\frac{\partial}{\partial\theta}\right)_{r,\phi} + \frac{1}{r^2\sin^2\theta}\left(\frac{\partial^2}{\partial\phi^2}\right)_{r,\theta} \\
&= (\text{terms depending only on } r) - \frac{1}{r^2}(\frac{\hat{L}^2}{\hbar^2})
\end{aligned} \tag{30}$$

This leads us to the angular part of the Hamiltonian,

$$\text{angular portion of } \hat{H} = \frac{-\hbar^2}{2m} \times \frac{-\hat{L}^2}{\hbar^2 r^2} = \frac{\hat{L}^2}{2I} \tag{31}$$

The angular momentum operator

The linear momentum operators are commutative due what they describe which is linear motion. But the angular momentum operators do not as they are products of both position and momentum. While the angular momentum in the classical sense relates to rotations in 3d space.

The classical angular momentum can be given as the dor product of the position and momentum as follows

$$\hat{\mathbf{L}} = \hat{\mathbf{r}} \times \hat{\mathbf{p}} \tag{32}$$

$$\begin{aligned}
&= (x, y, z) \times (p_x, p_y, p_z) = \begin{vmatrix} \mathbf{i} & \mathbf{j} & \mathbf{k} \\ x & y & z \\ p_x & p_y & p_z \end{vmatrix} \\
&= (yp_z - zp_y)\mathbf{i} + (zp_x - xp_z)\mathbf{j} + (xp_y - yp_x)\mathbf{k} \qquad (33) \\
&= (L_x, L_y, L_z)
\end{aligned}$$

Next, we can loosely apply the correspondence between the classical linear momentum and quantum mechanical linear momentum by replacing $\mathbf{p}$ with $-i\hbar\vec{\nabla}$ so equation (32) then becomes

$$\hat{\mathbf{L}} = -i\hbar(\hat{\mathbf{r}} \times \vec{\nabla}) \qquad (34)$$

And so we obtain the following:

$$\begin{aligned}
\hat{L}_x &= -i\hbar\left(y\frac{\partial}{\partial z} - z\frac{\partial}{\partial y}\right) \\
\hat{L}_y &= -i\hbar\left(z\frac{\partial}{\partial x} - x\frac{\partial}{\partial z}\right) \qquad (35) \\
\hat{L}_z &= -i\hbar\left(x\frac{\partial}{\partial y} - y\frac{\partial}{\partial x}\right)
\end{aligned}$$

The angular momentum operators for each Cartesian component do not commute as can be shown by computing:

$$[\hat{L}_i, \hat{L}_j] = i\hbar\varepsilon_{ijk}\hat{L}_k \qquad (36)$$

Where *ijk* can be any ordering of *xyz* and the Levi-Civita symbol ε_{ijk} is +1 for even and -1 for odd permutations of these coordinates.

Through some straightforward but tedious partial differentiation, we can convert the linear operators to spherical coordinates.

Quantum Mechanics in 3D

In 3D the Hamiltonian for rigid rotation is still simply the angular part of the Laplacian, because the radius remains fixed and there is no central potential.

$$\hat{H}_{rot} = \frac{\hbar^2}{2\mu r^2}\left[\frac{1}{\sin\theta}\frac{\partial}{\partial\theta}\left(\sin\theta\frac{\partial}{\partial\theta}\right)+\frac{1}{\sin^2\theta}\frac{\partial^2}{\partial\phi^2}\right] \tag{37}$$

The Hamiltonian of equation (37) has eigenfunctions which can be obtained from the Schrödinger equation by separation of variables:

$$f = Y(\theta,\phi) = \Theta(\theta)\Phi(\phi) \tag{38}$$

After the analysis of the wavefunction in the S.E. we obtain a differential expression in θ not discussed here and the following very familiar expression:

$$\frac{1}{\Phi(\phi)}\frac{d^2\Phi(\phi)}{d\phi^2} = -m_l^2 \tag{39}$$

This harkens back to the quantization of the rotational energy for 2D rotation except that the double degeneracy of the orbitals becomes a (2*l*+1)-fold degeneracy dictated by the requirement that

$$m_l = -l, -(l-1), -(l-2), \ldots, 0, \ \ldots, (l-2), (l-1), l \tag{40}$$

That is, the state described by a l quantum number is comprised of $(2l+1)$ substates of equal energy thus degeneracy.

Spherical Harmonics

The eigenfunctions of the 3D rigid rotor are the spherical harmonics labled by the quantum numbers *l* and m_l with corresponding energies

$$Y(\theta,\phi) = Y_l^{m_l}(\theta,\phi) = \Theta_l^{m_l}(\theta)\Phi_{m_l}(\phi) \tag{41}$$

$$E_l = \frac{\hbar^2}{2I} l(l+1) \tag{42}$$

All of the m_l states of a 3D rotor have the same energy E_l in the absence of a magnetic field. They are distinguished by the magnitude of the z component of the angular momentum.

Quantization of angular momentum

Various characteristics of the atomic orbitals depend on the quantum number l and m_l values associated for example: shapes, directional properties, degeneracy of atomic orbitals.

The energy for the three-dimensional rigid rotor.

$$E_{tot} = \frac{l^2}{2I} \Rightarrow \hat{H} = \frac{\hat{l}^2}{2I} \tag{43}$$

Therefore, both operators have a common set of eigenfunctions. So the operators should commute. Upon comparison, in (43), we can see that the only difference between the result of having the Hamiltonian and the angular momentum operator act on the spherical harmonic is the constant of 1/(2I) and this is shown in

$$\left[\hat{H}, \hat{l}^2\right] = 0 \tag{44}$$

The calculated, and measurable, angular momentum quantity (of precise eigenvalues) is that of

$$|l| = \hbar(\sqrt{l(l+1)}) \tag{45}$$

Connecting the dots: How classical mechanics corresponds to quantum mechanics

It has been presented that the correspondence principle links the classical theory to quantum theory. We can also present that the de Broglie relation [27] which proposes that light behaves as both a wave and a particle and with a relation via Planck’s constant allows for the connection of the free particle to the rotation on a ring.

$$p = \frac{h}{\lambda} \tag{46}$$

This particle traveling on a ring. Has a frequency of 2π, a radius of *r*, and a value equal to Planck’s constant times an integer multiple. We can make the relation from equation (46) to state that the mass of the particle time of the frequency and radius is equal to a multiple integer of $\hbar$.

This sets the stage for the discussion of quantization of energy states and the Schrödinger Equation. Since the functions, we use to describe the motion around are essentially wave equations. Though in the classical sense they will have no restriction on angular momentum (l) or energy (E). The waves must be in phase to increase in magnitude rather than be incrementally reduced to zero due to deconstructive overlap.

If we refer to Figure 3 we notice that the no matter how we approach the rotation of the molecule it rotates in two axes and does not rotate in the third axis. This allows us to state that the potential energy of the molecule is zero due to rotation about fixed length r. We can then state that the total energy of the system reduces to just the kinetic energy.

$$\begin{aligned} E_{tot,rot} &= KE + PE \\ &= T + V(x, y) \\ &= \frac{p^2}{2\mu} + 0 \end{aligned} \tag{47}$$

And for every classical observable, we have a corresponding linear operator. The quantum mechanical operator the for the total energy of the system is the Hamiltonian, $\hat{H}$. Much like (47) since potential energy of the system is zero. Therefore, we can make some simplifications for the 2D system.

$$\begin{aligned}\hat{H} &= \hat{T} + \hat{V} \\ &= \frac{\hat{p}^2}{2\mu} + 0 \\ &= \frac{-\hbar^2}{2\mu}\left(\frac{\partial^2}{\partial x^2} + \frac{\partial^2}{\partial y^2}\right)\end{aligned} \tag{48}$$

We’ve come all this way to finally mention the advancement and the shaping of how we can describe the quantum mechanical system the Schrödinger equation.

$$\hat{H}\Psi = E\Psi \tag{49}$$

And from (48) we can evaluate the following

$$\frac{-\hbar^2}{2\mu}\left(\frac{\partial^2\Psi(x,y)}{\partial x^2} + \frac{\partial^2\Psi(x,y)}{\partial y^2}\right) = E\Psi(x,y) \tag{50}$$

The right-hand side of the equations are the rotational eigenfunctions of the wave equation.

The Laplacian and coordinate systems

As you can imagine most molecules are not of the linear type and are asymmetrical with respect to their mass distribution. So, the two-dimensional analysis presented in the previous section needs to be expanded to include this asymmetry and a third dimension, z. So, the Hamiltonian is expanded to accommodate this additional parameter.

$$\nabla^2 = \frac{-\hbar^2}{2\mu}\left(\frac{\partial^2\Psi(x,y,z)}{\partial x^2} + \frac{\partial^2\Psi(x,y,z)}{\partial y^2} + \frac{\partial^2\Psi(x,y,z)}{\partial z^2}\right) = E\Psi(x,y,z) \tag{51}$$

The Laplacian operator is a second order differential operator in the *n*-dimensional Euclidean-space, defined as the divergence ∇ of the gradient (∇f). Another change we can introduce is the use of the spherical coordinates system. This conversion from the cartesian system is then implemented in order to reduce the complexity to find a solution.

Rigid rotor and selection rules

We have introduced various parts of the rigid rotor model. And how do we fit this all together? With the conversion from Cartesian to spherical coordinates the second order differential equation which is now dependent on two variables θ and φ that can be separated, via the method of separation of variables, and we obtain the following relation where $\Phi(\theta)$ is the rotational eigenfunction.

$$\frac{-\hbar^2}{2\mu r^2}\frac{d\Phi(\theta)}{d\phi^2} = E\Phi(\phi) \tag{52}$$

With correspondence in mind, the energy in equation (52) can now be substituted with the information from Table 1.

$$\hat{T} = \frac{1}{2}I\omega^2 = \frac{\hat{l}^2}{2} \tag{53}$$

The difference in energy between levels that is observed because of either absorption or emission and can be described using equation (55). As discussed previously the necessity for the molecule of interest to have a permanent dipole or have a way to induce a permanent dipole as with the Stark effect is essential. [28]

So far we have been using the convention of l as angular momentum and this label is applied to atoms. As a matter of convention the J label is applied to the angular momentum of molecules and is the label that we will be using henceforth.

The selection rule for the rotation of a molecule is

$$\Delta J = \pm 1 \tag{54}$$

And the energy difference between adjacent states is

$$\begin{aligned}\Delta E = E_{J+1} - E_J &= \frac{\hbar^2}{2I}\left[(J+1)(J+2) - J(J+1)\right] \\ &= \frac{\hbar^2}{2I}(J+1) = \frac{\hbar^2}{4\pi^2 I}(J+1)\end{aligned} \tag{55}$$

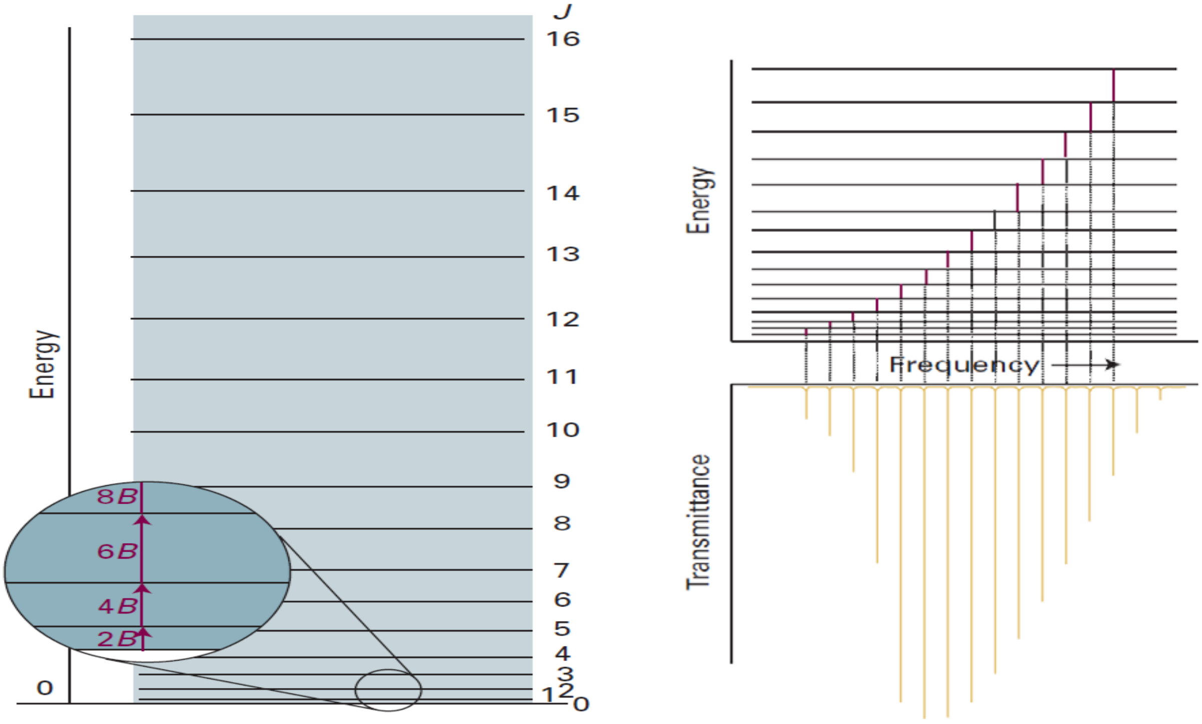

Figure 6: For a linear or symmetric molecule the increase in energy for each transition is equivalent to 2B. (left panel) Increase in energy, 2B, should correspond to an emission signal. (right panel) [29]

The change in notation is subtle. But the J term is used to denote that the rotation is relative the body of a molecule where, l, is relative to an electron or free particle. We can then use the Bohr relation to show at which frequency the absorption transitions occur.

$$v = \frac{\hbar^2}{2I}(J+1) \qquad J = 0,1,2,\ldots \tag{56}$$

Though usually, we write equation (56) as

$$v = 2B(J+1) \qquad J = 0,1,2,\ldots \tag{57}$$

And

$$B = \frac{h}{8\pi^2 I} \qquad (Hz) \tag{58}$$

is called the rotational constant of the molecule and was commonly expressed in wavenumbers (cm^{-1}) and we can convert by using the relation, $\overline{v} = \frac{v}{c}$ so equation (58) becomes

$$\overline{v} = 2\overline{B}(J+1) \qquad J = 0,1,2,... \tag{59}$$

And the rotational constant when it is expressed in wavenumbers.

$$\overline{B} = \frac{h}{8\pi^2 I} \qquad (cm^{-1}) \tag{60}$$

The Figure 8 demonstrates that the rigid rotator model predicts the microwave spectrum of a diatomic molecule to consist of a series of equally spaced lines with a separation of $2\overline{B}$. The regular spacing is a great tool to help understand what's happening in the absorption of the microwave energy and the subsequent rotation of the molecule. However, as we explain below for most molecules we have to integrate a correction into the analysis.

Centrifugal distortion and the Semirigid rotor

The perturbation of a real structure must be accounted for when presenting experimental results. In Figure 8 this is not considered and instead only represents the ideal condition. The experimental spectra exhibit a discrepancy when compared to calculated spectra and so a correction factor in the effective Hamiltonian for the calculated spectra must be included to account for this offset. This shift in real spectra and is not very large for a symmetric molecule, but it does contribute significantly to asymmetric molecules during the assignment of the spectra. The shift is observed for all observation but is most noticeable where large transitions may occur due to large angular momentum and very large rotational energies.

Rovibrational energy of non-rigid rotor:

$$E_{n,J} = h\nu\left(n+\frac{1}{2}\right) + B_e J(J+1) - \alpha_e\left(n+\frac{1}{2}\right) - DJ^2(\mathrm{J}+1)^2$$

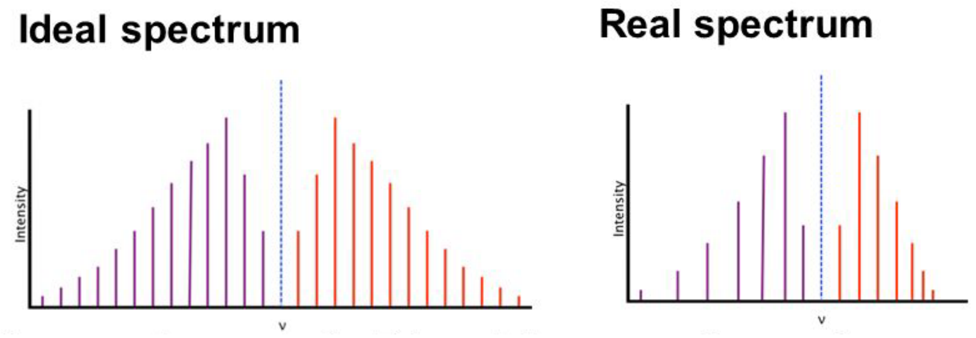
Ideal spectrum

Real spectrum

Figure 7: As energy increases, the R-branch lines move closer and as energy decreases, the P-branch lines move farther apart, this is attributable to two phenomena: rotational-vibrational coupling and centrifugal distortion.

Tops

When talking about rotational spectroscopy, the symmetry of the molecule plays a significant role in the spectra that will be observed. Because we can delve into an ocean of information this section will be concise enough to allow the reader to be able to have an idea of what’s going on. We use group theory to describe the symmetry of a molecule. The designation of a molecules symmetry can help us evaluate whether an overall dipole exists in a molecule. And as we are not talking about static models but rather molecules rotating through three-dimensional space the natural phenomenon that play a role are to be described.

We can assign a main axis of rotation to be at the center of mass and is rotated so that the moment of inertia tensor is diagonal. This process works for a rigid molecule. And so we obtain three moments of inertia, I, relative to *x*, *y*, and *z*. We can use these labels to assign molecules to four different types of tops.

Tops	Moments of Inertia	Examples
Linear (which include diatomics)	$I_x = I_y ; I_z = 0$	HCCH
Spherical	$I_x = I_y = I_z$	CH_4, SF_6
Symmetric	$I_x = I_y \neq I_z$	BF_3, CH_3Cl
Asymmetric	$I_x \neq I_y \neq I_z$	H_2O,CH_3OH

As referenced in a previous section it is easiest to assign an internal frame of reference separate from the laboratory reference axis of *x*,*y*,*z* and assign these with respect to the magnitude of the moments of inertia. This internal coordinate system designated as *a*,*b*,*c* and the moments of inertia is assigned from largest to smallest with the *A* axis being largest and *C* axis smallest in magnitude.

Top	Moments of Inertia	Examples
Linear (which include diatomics)	$I_A = I_B ; I_C = 0$	HCCH
Spherical	$I_A = I_B = I_C$	CH_4, SF_6
Prolate Symmetric	$I_A < I_B = I_C$	CH_3Cl
Oblate Symmetric	$I_A = I_B < I_C$	BF_3
Asymmetric	$I_A \neq I_B \neq I_C$	H_2O

All of the molecules in this thesis are asymmetric and so the following discussion will entirely with information regarding these molecules.

In general there is not a level formula available for symmetric and spherical tops. The rigid rotor Hamiltonian:

$$\hat{H} = A\hat{J}_a^2 + B\hat{J}_b^2 + C\hat{J}_c^2 \tag{61}$$

Commutes with J^2 and J_z in the laboratory coordinate system so that *J* and M_J remain good quantum numbers. However, the Hamiltonian does not commute with the components (J_a, J_b, J_c) in the molecular coordinate system. This means that the 2-fold degeneracy of K- in the symmetric tops is lifted and *J* splits into 2J+1 components. The case of an asymmetric top the levels are labeled by an index $\tau = J, ..., 0, ..., -J$ in order of decreasing symmetry. The energy levels of the asymmetric top are most easily derived using symmetric top basis functions. First deriving the matrix elements of $\hat{H}$ and then diagonalizing $\hat{H}$ to find the energy eigenvalues and eigenvectors. For each value of J, a $(2J+1)\times(2J+1)$ matrix results and the $2J+1$ eigenvalues are easily labeled by τ.

The degree of asymmetry for a molecule is determined by the asymmetry parameter, κ:

$$\kappa = \frac{2B - A - C}{A - C} \tag{62}$$

Values of κ range from -1 for a prolate top and +1 for an oblate top and a symmetric top will have a value of 0.

The selection rules for asymmetric tops depend on the dipole moments of the molecule with respect to the principal molecular axis μ_a, μ_b, μ_c which are components of the overall dipole moment vector $\vec{\mu}$.

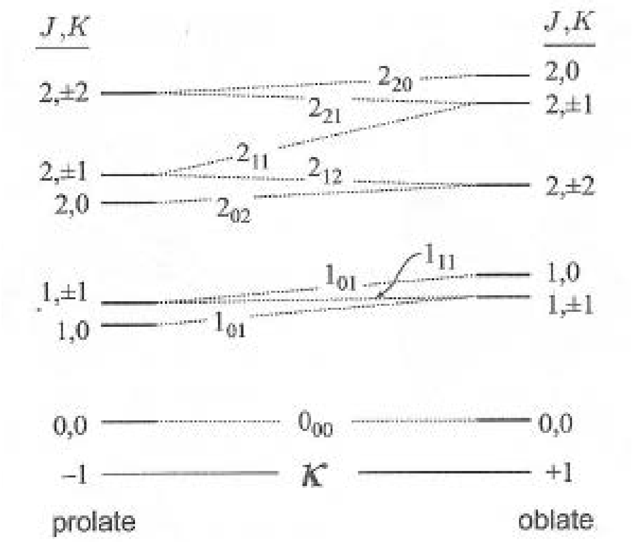

Figure 8. The selection rules can be divided into three general cases [30]:

1. a-type transitions when $\mu_a \neq 0, \Delta K_a = \pm 0(\pm 2, \pm 4, ...),\ \Delta K_c = \pm 1(\pm 3, \pm 5, ...)$
2. b-type transitions when $\mu_b \neq 0, \Delta K_a = \pm 1(\pm 3, ...),\ \Delta K_c = \pm 1(\pm 3, ...)$
3. c-type transitions when $\mu_c \neq 0, \Delta K_a = \pm 1(\pm 3, \pm 5, ...),\ \Delta K_c = \pm 0(\pm 2, \pm 4, ...)$

The transitions in parentheses are weaker than the main transitions. A molecule of low symmetry can have all three components, not equal zero, $\mu_a \neq \mu_b \neq \mu_c \neq 0$, and so they would show up in the rotational spectrum.

Time-independent Schrödinger equation

This section demonstrates that the time-dependence of Ψ is trivial for the spatial and time parts being separable and is an eigenfunction of the Hamiltonian.

We consider the Time-Dependent Schrödinger Equation (TDSE).

$$\widehat{\mathrm{H}}\Psi = i\hbar\frac{\partial \Psi}{\partial t} \tag{63}$$

The postulates of quantum mechanics are presented by McQuarrie in his book Quantum Chemistry [31]. Postulates 1 & 5 state, respectively, that a quantum mechanical system is completely specified by a function $\Psi_n(\vec{r}, t)$ that evolves according to the time dependent

Schrodinger equations. The function, called the wave function or the state function has the important property that $\Psi^*(\vec{r},t)\Psi(\vec{r},t)\,dx\,dy\,dz$ is the probability that the particle lies in the volume element $dxdydz$ located at $\vec{r}$, at the time, *t*.

For most systems, the Hamiltonian operator does not contain time explicitly. We can then apply the method of separation of variables and write:

$$\Psi(x,t) = \psi(x)\,f(t) \tag{64}$$

By substituting (64) into (63) we obtain

$$\hat{H}(\psi(x)\,f(t)) = i\hbar\frac{\partial(\psi(x)\,f(t))}{\partial t} \tag{65}$$

After some rearrangement, we can separate the variables so the sides are only a function of x or t.

$$\frac{1}{\psi(x)}\hat{H}\psi(x) = \frac{i\hbar}{f(t)}\frac{df}{dt} \tag{66}$$

But this means that we need an equivalence constant as the left side of the equation exists in position and the right-hand side is only in time. Therefore, we make two assumptions first that we call the constant needed as E and that gives us the time-independent Schrödinger equation.

$$\hat{H}\Psi(x) = E\psi(x) \tag{67}$$

We also obtain

$$\frac{df}{dt} = -\frac{i}{\hbar}E\,f(t) \tag{68}$$

with easily verifiable solution

$$\Psi(x,t) = \psi(x)e^{\frac{-iEt}{\hbar}} \tag{69}$$

This expression only changes by a phase factor of constant magnitude. If we substitute $E = hv = \hbar\omega$ into equation (70) another relationship is obtained.

$$\Psi(x,t) = \psi(x)e^{-i\omega t} \tag{70}$$

If the system we are looking at is in an Eigenstate as defined by (70) then

$$\left|\Psi_n\right|^2 = \Psi_n^*(x,t)\Psi_n(x,t) = \psi_n^*(x)e^{i\omega t}\psi_n(x)e^{-i\omega t} = \left|\psi_n(x)\right|^2 \tag{71}$$

So, the calculated averages and the probability densities are independent of time and the $\psi_n(x)$ are called stationary-state wave functions. This lays the whole premise for transitions in molecules and atoms as the spectroscopic characteristics of the systems are described as the transitions from one stationary state to another.

Electronic structure calculation

Method of steepest descent

In this case the potential energy surface of the system is being analyzed at different geometries in order to find the most stable, lowest energy, form of the molecule. This of course can produce enermous amounts of information depending on the granularity of your search. The method of steepest descent evaluates the second partial derivative of the function. Because we can have molecular geometries of lower relative energy the method of steepest ascent can be flawed. But it is a great starting point in evaluating molecular systems. In mathematical terms it’s presented as the following:

An algorithm for finding the nearest local minimum of a function which presupposes that the gradient of the function can be computed. The method of steepest descent, also called the gradient descent method, starts at a point P_0 and, as many times as needed, moves from P_i to $\mathrm{P}_{\mathrm{i}+1}$

by minimizing along the line extending from P_0 in the direction of $-\nabla f(P_0)$, the local downhill gradient. The number of steps or iterations needed to find the minima is determined by the end user but the goal is to locate the point where the gradient of the function is minimized.

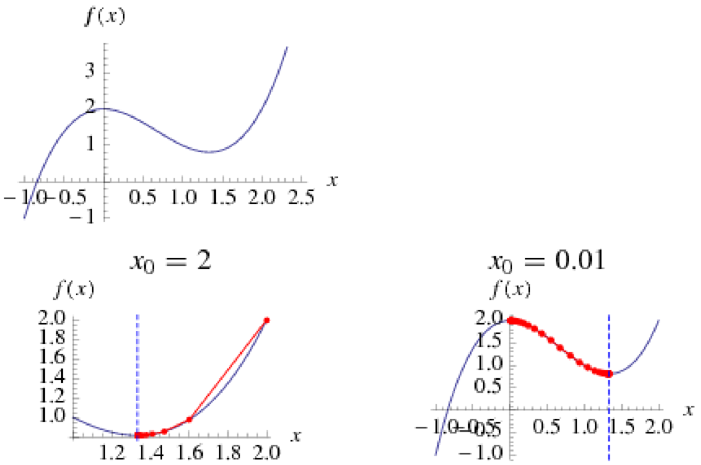

$x_0 = 2$

$x_0 = 0.01$

Figure 9: Example of the method of steepest descent. [32]

When applied to a 1-dimensional function $f(x)$, the method takes the form of iterating $x_i = x_{i-1} - \varepsilon f'(x_{i-1})$ from a starting point x_0 for some small $\varepsilon > 0$ until a fixed point is reached. The results are illustrated above for the function $f(x) = x^3 - 2x^2 + 2$ with $\varepsilon = 0.1$ and starting points $x_0 = 2$ and 0.01, respectively. This method has the severe drawback of requiring a great many iterations for functions which have long, narrow valley structures. In such cases, a conjugate gradient method is preferable. Which is an interative method that is used to solve unconstrained optimization of energy surfaces. [32]

Ab initio molecular orbital theory

Molecular orbital theory is an approach to molecular quantum mechanics problems where one-electron functions called orbitals are used to approximate the full wave functions. *Ab-initio* calculations model the wavefunctions using only the fundamental constant the atomic number of the nuclei. A molecular orbital is a function of the Cartesian coordinates of the electron

$\psi(x,y,z)$. And the square of the molecular orbital ψ^2, (or $|\psi|^2$ if ψ is complex), is regarded as the probability distribution of the electron in Cartesian space. In addition to the Cartesian coordinates, electronic spin must be considered in the electronic distribution and can assume values of $m_s = \pm\frac{1}{2}$; the resulting functions are spin orbitals: the complete wavefunctions for the single electrons $\psi(x,y,z)\alpha(\xi)$ or $\psi(x,y,z)\beta(\xi)$.

The molecular orbitals must be orthogonal:

$$S_{ij} = \int \psi_i^* \psi_j \, dx\, dy\, dz = 0 \text{ for } i \neq j \tag{72}$$

where S_{ij} is the overlap integral and ψ_i^* is the complex conjugate. The orbitals are also normalized, that is, the probability of finding an electron anywhere in space is unity:

$$S_{ij} = \int \psi_i^* \psi_j \, dx\, dy\, dz = 1 \tag{73}$$

The full molecular orbital wavefunction for a closed-shell ground state n-electron system with $n/2$ double occupied orbitals, Ψ, is built from the spin orbitals with a Slater determinant:

$$\Psi = \frac{1}{\sqrt{n!}} \begin{vmatrix} \psi_1(1)\alpha(1) & \psi_1(1)\alpha(1) & \psi_2(1)\alpha(1) & \cdots & \psi_{n/2}(1)\beta(1) \\ \psi_{n/2}(1)\beta(1) & \psi_{n/2}(1)\beta(1) & \psi_2(2)\alpha(2) & \cdots & \psi_{n/2}(2)\beta(2) \\ \vdots & \vdots & \vdots & \ddots & \vdots \\ \psi_1(n)\alpha(n) & \psi_1(n)\beta(n) & \psi_2(n)\alpha(n) & \cdots & \psi_{n/2}(n)\beta(n) \end{vmatrix} \tag{74}$$

Where the molecular orbitals ψ_i are built from a set of one-electron functions called basis functions:

$$\psi_i = \sum_{\mu=1}^{N} c_{\mu i} \phi_\mu \tag{75}$$

Dispersion correction

Density Functional Theory as an evolution of Hartree-Fock theory has some drawbacks. Some of these drawbacks include the treatment of the exchange interaction. The correct functional to treat exchange is not known and instead a semi-empirical method is used to make approximations. For one of the projects later in this thesis a functional form is used in order to try and compensate for the drawback of intramolecular dispersion effects and in 2011 Grimme et. al.[33] presented a paper detailing the modifications that could be applied to some of the DFT functionals for dispersion effects regarding dispersion energies.

Electron correlation

This work uses Møller–Plesset perturbation theory to incorporated electron correlation in electronic structure calculations. The difference in energy between the exact energy of the wavefunction and then energy obtained using Hartree–Fock methods is the correlation energy. Møller–Plesset perturbation theory is used to find the correlation energy by applying a perturbation to the zero-order electronic Hamiltonian, $\mathscr{H}^0$**,** forming the correlation energy by applying a perturbation to a zero-order Hamiltonian is the sum of the one-electron Fock operators as defined below:

$$\mathscr{H}^0 = \sum_i^n \hat{f}_i. \tag{76}$$

The perturbation $\mathscr{H}^{(1)}$ is given by:

$$\mathscr{H}^{(1)} = \mathscr{H}^{elec} - \sum_i^n \hat{f}_i. \tag{77}$$

Thus the ground state Hartree-Fock energy E_{HF} of a normalized wavefunction Ψ_0 is:

$$E_{HF} = \left\langle \Psi_0 \middle| \mathscr{H}^{elec} \middle| \Psi_1 \right\rangle = \left\langle \Psi_0 \middle| \mathscr{H}^{(0)} + \mathscr{H}^{(1)} \middle| \Psi_1 \right\rangle \tag{78}$$

And the correction to the Hartree-Fock energy is the second-order perturbation.

The second-order perturbation is given by:

$$E^{(2)} = \sum_{J \neq 0} \frac{\left\langle \Psi_J \middle| \mathscr{H}^{(1)} \middle| \Psi_0 \right\rangle \left\langle \Psi_0 \middle| \mathscr{H}^{(1)} \middle| \Psi_J \right\rangle}{E_0^{(0)} - E_J^{(0)}} \tag{79}$$

Where Ψ_J is a multiply excited wavefunction that is an eigenfunction of $\mathscr{H}^0$ with an eigenvalue of $E_J^{(0)}$. The inclusion of this second-order correction to energies is second-order Møller–Plesset perturbation theory (MP2).

CHAPTER III

INSTRUMENTATION

History of microwave spectroscopy

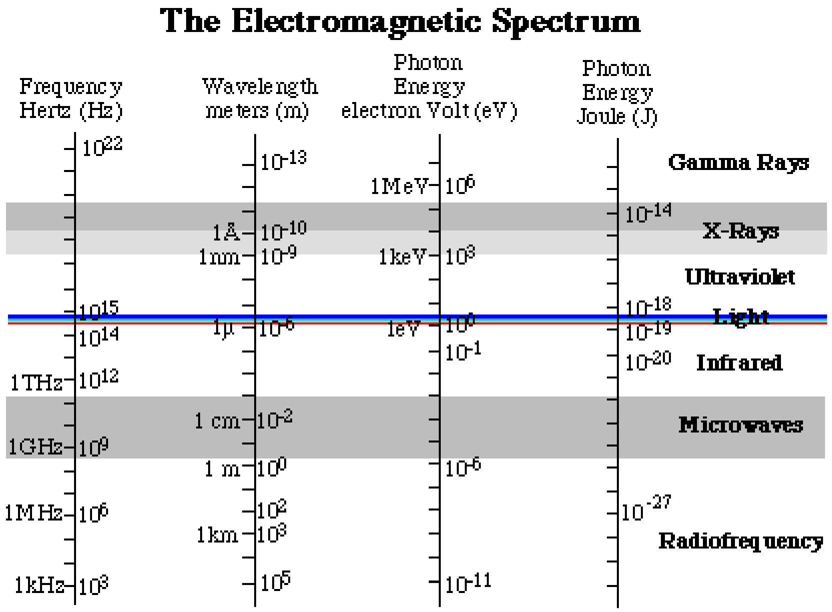

Unit Abbreviations:

THz	terahertz	Å	Angstrom	MeV	Mega electron volts
GHz	gigahertz	nm	nanometer	keV	kilo electron volts
MHz	megahertz	µm	micrometer		
kHz	kilohertz	cm	centimeter		
		km	kilometer		

Figure 10: Electromagnetic (EM) spectrum.

We should start from somewhere and referencing the electromagnetic spectrum (EM) is a great place to start! Why here? Because as you excite an analyte with energy, depending on the wavelength that is being absorbed and the structure of the molecule, different excitations will be observed. Electron transitions in atoms and molecules produce spectra in the visible and ultraviolet range. When vibrational motions of atoms are considered, the region of the EM that they would be observed in the infrared region. For this thesis, the region that bears the most interest for the studies of the molecules that are presented reside in the microwave (MW) region of the EM. This region provides insight into the still slower end-over-end rotation of molecules which have characteristic energy frequencies so low that they exist in the MW region and dominate MW spectra.[9]

Region	Frequency (Hz)	Wavelength (m)	Wavenumber (cm^{-1})	Energy ($Jmolecule^{-1}$)	Molecular Process
Microwave	10^9-10^{11}	$3.0x10^{-1}$-$3.0x10^{-3}$	0.033-3.3	$6.6x10^{-25}$-$6.6x10^{-23}$	Rotation of Polyatomic Molecules
Far Infrared	10^{11}-10^{13}	$3.0x10^{-3}$-$3.0x10^{-5}$	3.3-330	$6.6x10^{-23}$- $6.6x10^{-21}$	Rotation of Small Molecules
Infrared	10^{13}-10^{14}	$3.0x10^{-5}$-$3.0x10^{-6}$	330-3300	$6.6x10^{-21}$- $6.6x10^{-20}$	Vibration of flexible bonds
Visible & Ultraviolet	10^{14}-10^{16}	$3.0x10^{-6}$-$3.0x10^{-8}$	3300-$3.3x10^{-5}$	$6.6x10^{-20}$- $6.6x10^{-18}$	Electronic Transitions

Table 2: Portion of the electromagnetic spectrum and the molecular processes that result of the excitation in each respective band. Adapted from McQuarrie. [1]

After World War II Walter Gordy [34] presented a thorough paper on the state of MW spectroscopy up to that point. But as he mentioned in that paper the first pre-war experiment was conducted on ammonia in the “centimeter” range by Cleeton and Williams. [35] The limiting factor for the analysis of chemicals up until that point was the lack of vacuum tubes that could generate waves in the desired range. This was later overcome due to the necessity for a better radar system and the need for a large production volume. The item that would eventually give the desired frequency range, which was the second-generation magnetron, was brought over by the British in the early 1940s. After undergoing review, the research of this device was placed into the hands of the newly created Radiation Lab at the Massachusetts Institute of Technology in Boston, Massachusetts. Due to restrictions related to World War II the magnetron did not make much headway into many research labs until after 1945

Microwave spectroscopy has provided a rich and diverse amount of information over the last 70 years. During that time, there have been several revolutions in the field. . But three revolutions must be acknowledged. Initially, MW spectrometers needed a large amount of space to lay out the waveguide, which were box-like or tubular cavities, of certain dimensions that corresponded to the bandwidth that was being investigated. Later the idea that a cavity of modest size could be modified to perform the job of the space-consuming waveguides. Thus, decreasing the footprint from taking up a large portion of the lab to roughly six sq.ft.

FTMW spectrometer

In 1976 W.H. Flygare [36] published the application of Fourier-transform to the data collected from a microwave spectrometer. Then Balle and Flygare developed and subsequently published the development of Fabrey-Perot based MW spectrometer [37]. This improvement to the design of the MW spectrometer led to the increased ease of use and ability to analyze molecules. This mature form of the spectrometer stayed in use for decades. Improvements to the systems were mostly due to the evolution of electronics. Eventually, this lead to the most recent revolution which occurred in 2008 by the Pate group at the University of Virginia.[38] Their paper evolved the field by advancing the single frequency determination of the Flygare-Balle cavity, and subsequent resonance of ± 0.5 MHz around that frequency, based Fourier-transform microwave spectrometer and added a chirped-pulse that flooded the frequency spectrum that the cavity was tuned for. This practically and effectively cut down the collection of data for a new molecule or molecular system by orders of magnitude. Previously the sampling of a molecule would take many weeks or months could to take even longer to assign the spectra of a single molecule. The chirped-pulse Fourier-transform microwave spectrometer (CP-FTMW) could do a similar analysis in the frequency range of interest and the time it would take to collect the data could be as little as a day(s) or a week(s). Depending on the frequency range being analyzed were large enough and the complexity of the molecular system..

Cavity based Fourier transform microwave spectroscopy

In MW spectroscopy, there are two parts of the instrument: the electronic and the mechanical. Since a FTMW spectrometer is not a common instrument the general schema for both parts will be presented. The microwave synthesizer can be though of as the lifeblood of the instrument. And through recent advances, this integral piece has reduced in cost by a significant margin and can be replaced by a CMOS electronic board at a fraction of the cost [39]. This device produces the energy required to excite the analyte and this energy is split by a power divider.

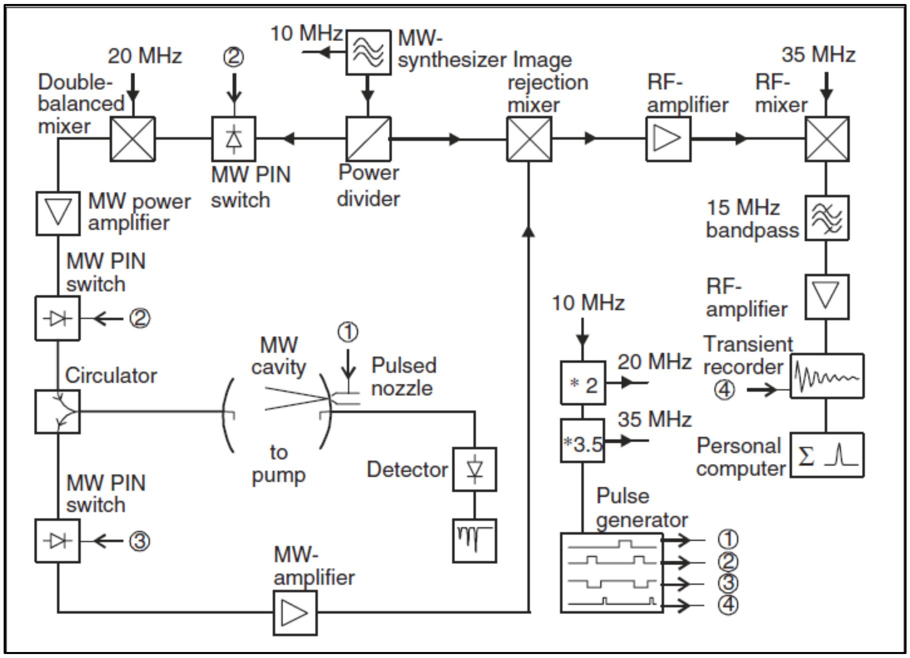

Figure 11: Simplified diagram of a FTMW spectrometer.[40]

One feed is augmented by sideband modulator that adds an additional frequency to the signal going to the microwave chamber. The addition of the 20 MHz side band is to ensure that the resonant ringing in the cavity due to the microwave pulse and any spurious noise from the signal's propagation is neglected. The sideband addition is done to ensure that the FID is not lost in the noise. This pathway is controlled by a MW pin switch that opens at an interval set by the user but is usually only a few microseconds in duration. Care must be taken that this pulse is not too long because this may result in the damaging of the detection circuit. The signal is fed into the chamber by a simple antenna on one side and a receiving antenna on the opposite side. The sample chamber as described elegantly by Jaeger and Xu in the Encyclopedia of Inorganic Chemistry [41] as the "heart" of the instrument.

The vacuum chamber serves as the housing for both the Fabrey-Perot type system and the MW cavity sample chamber. The vacuum chamber is evacuated by a combination of a foreground pump, which reduces the pressure to a couple of Torr, and a diffusion pump to reach a background pressure in the 10^{-6} bar range. This process is known as pumping down the cavity. When the vacuum chamber is maintaining a consistent vacuum the sampling experiment may begin.

The compounds presented in this thesis were in the gaseous phase. But this is, by no means, a requirement. Various techniques can be utilized to observe the rovibrational spectrum of condensed phase samples. For example, to put a low vapor pressure component into the gaseous phase a sample warmer which consists of a heating element and wrap to keep the temperature at a consistent range can and was utilized, or cooling a sample with a Peltier cooler in order to faciliate the commingling with another sample in order to form a dimer complex before entering the vacuum chamber can and were done while visiting Dr. Kukolich's lab at the University of Arizona. [42] Also, running an electrical current through the sample or via laser ablation. These techniques are included so we are aware that there are additional methods of analysis possible in a microwave experiment.

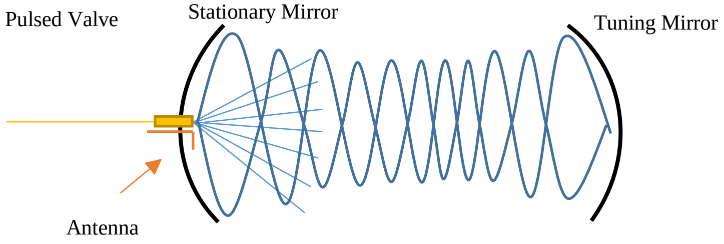

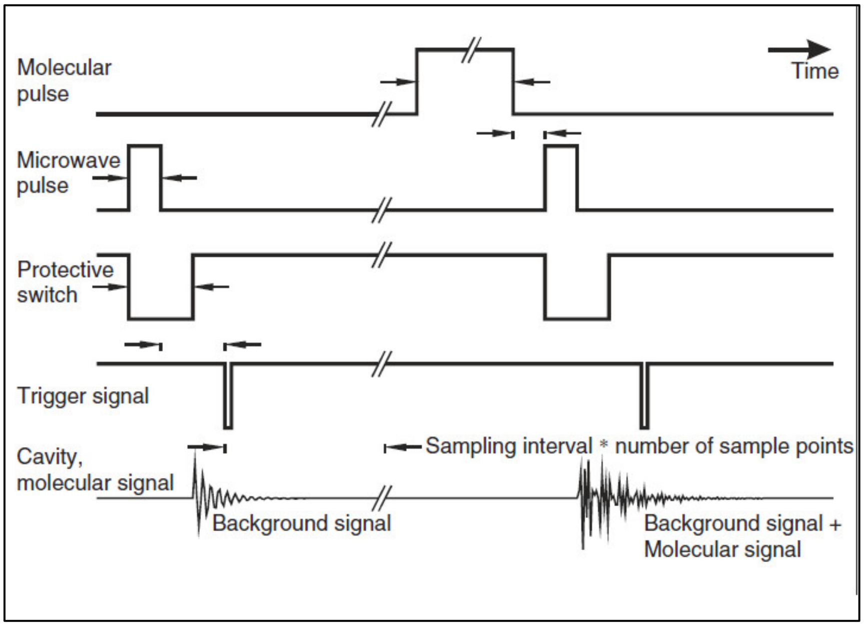

Figure 12: Scheme of the various relations of the microwave pulse.[40]

After the sample has entered the cavity and undergone supersonic expansion, it is bombarded by the MW signal and absorbs sufficient energy that it is excited to a higher energy state and after the cessation of the signal. The excited sample returns to the ground state and the emission signal is captured by the receiving antenna. So, the emission signal, the MW signal, and the additional sideband modulation is fed into a low noise MW amplifier and then into an image rejection mixer. After this, the molecular emission signal and the sideband modulation are recorded by a computer program and then converted by Fourier-transform to take the free induction decay (FID) from the molecular emission in the time domain into the frequency domain.

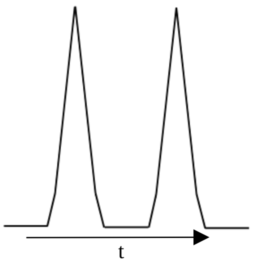

Figure 13: Doublet due to Doppler broadening.

The sampling continues at a single frequency for a reasonable time and this varies depending on the strength of the emission signal and the resolution that is desired. Each FID returns a single frequency and each sampling may take several “snapshots” which are then averaged and as a result increase the signal to noise ratio. As mentioned previously in this thesis the time required for a single experiment can vary greatly depending on several factors which must include the molecule itself, the type of spectrometer, and the frequency range of interest. Though with the addition of automation to a FTMW: the stepping which is incremental progress across the spectrum range of interest, tuning of the cavity, and recording of data can be done without intervention over GHz ranges.

Chirped-pulse FTMW

The Balle-Flygare MW spectrometer has been the standard technique for many years. The constant evolution of electronics and refinement of the cavity based technique has served the community excellently. In this section, we talk about the last major evolution of the microwave community which was introduced in 2006 by the Pate group at the University of Virginia and subsequently published in 2008.[38] This technique needed advances in two integral pieces: the ultrafast oscilloscope and the capability to digitally create microwaves.

This next evolution in the microwave technique has introduced us to the chirped-pulse FTMW spectrometer. The fundamentals that govern a cavity based or chirped-pulse experiment are the same. The instrument does differ in the components and the overall collection of the MW spectrum when compared to the cavity based spectrometer.

We present a brief overview of both points in this section to familiarize the reader with the method in which some the results were obtained in later chapters.

The leap forward, in this case, was the speed in which a large bandwidth could be observed. A cavity FTMW uses a single frequency at a time per observation that was performed. When you consider that the average time per sampling takes about ten to fifteen minutes. Most of that time is spent in the adjustment of the mirrors and some on the collection of the data. So to fully analyze a molecule of interest could easily take weeks if not months.

The chirped pulse FTMW spectrometer on the other hand floods a large frequency range in a single instant. The desired range is swept with energy from an arbitrary waveform generator (AWG) which controls the sweep range, rate (pulse duration), and overall phase. This allows for the passing of the frequency sweep to pass through a microwave frequency multiplier. So, the pulse bandwidth is increased by the frequency of the multiplication factor and most importantly leaving the pulse duration unchanged. This enables the ability to increase the frequency range from a small bandwidth to a multiplied bandwidth (e.g., a 1.5 GHz bandwidth entering a x8 multiplier would increase the frequency range to roughly 12 GHz).

The other thing necessary for this technique to function correctly is the advancement of the digital oscilloscope and its internal component the ultrafast signal digitizer which collects the free induction decay signal in the time domain. The FID frequency domain is calculated by a fast Fourier transform of the molecular emission.

The chirped pulse MW spectrometer, in general, has three main components:

1. The chirped pulse microwave source.
2. The molecular beam spectrometer
3. The broadband receiver.

The following figure is from the Pate group and was published in 2006. [38]

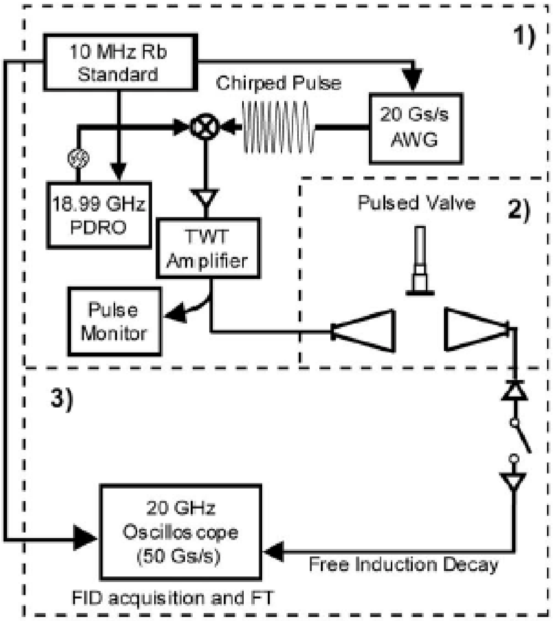

Figure 14: Schematic of the 11 GHz chirped-pulse Fourier transform microwave (CP-FTMW) spectrometer.

CHAPTER IV

ROTATIONAL SPECTROSCOPIC AND THEORETICAL STUDY OF THE PERFLUOROBUTYRIC ACID –FORMIC ACID COMPLEX

Introduction

Perfluorinated carboxylic acids (PFCAs) consist of a terminal carboxylic group and an alkyl chain which is fully fluorinated. PFCAs have been used as surfactants in industrial processes and also as ion-pairing agents in analytical chemistry [43]. PFCAs are known to be toxic and the effects of some longer chain PFCAs, for example perfluorooctanoic acid, on the environment have been extensively investigated by the United States Environmental Protection Agency (EPA) [6]. We note that perfluorooctanoic acid was recently included in the list of the Stockholm Convention on Persistent Organic Pollutants [44]. Perfluorobutyric acid (PFBA), a shorter chain PFCA, was identified as one of the several possible candidates [45] to replace perfluorooctanoic acid. However, these shorter chain PFCAs are more water soluble and might pose other serious environmental issues. Some of us have recently reported rotational spectroscopic studies of several short-chain PFCAs, such as perfluoropropionic acid [46], PFBA [7], and perfluoropentanoic acid , as well as their mono and/or dihydrates [45,47]. In this context, it is also of considerable interest to investigate structural properties of the hydrogen (H)-bonded complexes between PFBA and other simple acids, such as formic acid (FA), and with itself. Carboxylic acids have a strong tendency to dimerize or form larger aggregates even at room temperature [48] because of the favorable formation of strong intermolecular H-bonds. It is well known that the two carboxylic acid groups favor the formation of an eight-membered ring featuring two H-bonds [49]. Detection of rotational transitions requires the molecular system to be studied to have a permanent electric dipole moment and they can therefore not possess a center of symmetry. For this reason, many of the carboxylic acid dimers which have been studied with microwave spectroscopy are heterodimers which consist of two different acids. Since FA is the simplest carboxylic acid and has sufficient vapor pressure at room temperature, it is not surprising that many FA containing heterodimers with other carboxylic acids have been studied by using rotational spectroscopy. Some examples are propiolic acid—FA [11–13], benzoic acid—FA [15], and nitric acid—FA [50], where tunneling splittings due to a double proton transfer between the two acids were detected experimentally. The potential energy surfaces of these planar complexes have a double- minimum potential, similar to systems that undergo a single proton tunneling motion, such as malonaldehyde [51–54] and tropolone [55,56]. A generic double-minimum potential for a double proton transfer in planar molecules is shown in Fig. 22 with the equivalent minima indicated. Howard and co-workers [16] published a beautiful paper on acetic acid—FA, a ‘large’ nonrigid molecule, and showed how the double proton tunneling motion is strongly coupled to the methyl internal rotation. In that work, they also developed a suitable framework to extract meaningful spectroscopic constants, such as the principal moments of inertia and the methyl bond axis orientation from the experimental spectra. In other FA containing acid dimers, such as fluoro/difluoro/trifluoroacetic acid—FA [57–59], cyclopropanecarboxylic acid—FA [60], 3,3,3-trifluoro-2-(trifluoromethyl)propanoic acid—FA [61], and acrylic acid—FA [62], no splittings due to a double proton tunneling process were observed experimentally. In these systems, the double proton transfer would require a simultaneous CF_3 internal rotation (or other heavy group motions) to reach an equivalent potential energy minimum and the double proton tunneling is quenched. In the difluoroacetic acid—FA case [58], Caminati and co-workers observed some narrow splittings between 10 and 20 kHz, which may be attributed to either tunneling between the gauche +/- forms of difluoroacetic acid or double proton tunneling coupled to a simultaneous CHF_2 internal rotation in order to reach an equivalent potential energy minimum. They could attribute the splitting to gauche +/- tunneling of the difluoroacetic acid subunit by studying all three deuterated isotopologues and detecting splittings of similar magnitude in all spectra. Their conclusion is consistent with the proposal that the double proton transfer is quenched if a simultaneous heavy atom motion is required to reach an equivalent potential minimum. On the other hand, Obenchain et al. had recently recorded rotational spectra of the perfluoropropionic acid—FA complex [63] where each a-type rotational transition is split into a doublet, with spacings of less than 1 MHz. The exact origin of the observed splittings, however, is still unclear. It is therefore interesting to explore the closely related PFBA—FA heterodimer to obtain a more complete picture of double proton tunneling and the nature of the H-bonding interactions in these perfluorinated acid containing hetero acid dimers.

Fourier transform microwave spectroscopy (FTMW) has been used extensively to probe molecular structure and dynamics of small molecules and their non-covalently bound complexes in the gas phase [64,65].In recent years, it has been applied to studies of molecules [66] and complexes [67] of important environmental interest, some of which are discussed above [68]. In this paper, we report the first FTMW spectroscopic investigation of the PFBA—FA heterodimer, complemented by ab initio calculations. Both broadband chirped pulse FTMW [69,70] and cavity-based FTMW [71] spectrometers at the University of Alberta were utilized in the current study. The latter has a higher resolution capability than the former one. Our aim was not only to measure rotational transitions to extract structural properties of the acid heterodimer, but also to examine if there are any splittings associated with double proton transfer or other tunneling motions.

Theoretical and experimental methods

A computational search for low energy conformers of the PFBA—FA complex was carried out using the GAUSSIAN 09 package [2]. Geometry optimizations were performed using the second order Møller-Plesset perturbation (MP2) and the dispersion corrected density functional theory (DFT), B3LYP-D3BJ [33], methods. The 6-311++G(2d, p) basis set was used. Harmonic vibrational frequencies were also determined after geometry optimization to ensure that the optimized structures are true minima.

Initial searches for rotational transitions of the PFBA—FA complex were carried out using the chirped pulse FTMW spectrometer; the experimental details of this spectrometer had been reported previously [60,61]. All final frequencies were measured with the cavity-based FTMW spectrometer [62] in the region from 7 to 18 GHz. Helium or neon gas mixed with 0.2% FA was bubbled through a sample reservoir containing PFBA, which was situated right before the pulsed nozzle, for both the chirped pulse scans and the final cavity-based measurements, respectively. FA (99%, Sigma Aldrich), PFBA (99%, Alfa Aesar), and helium/neon (99.9990%) were used without further purification.

Results and discussion

Two conformers of the PFBA monomer were predicted theoretically, although the second conformer is significantly less stable and had not been detected experimentally [7]. The MP2 conformational search located six low energy conformers for the PFBA—FA heterodimer.

Similar results were obtained at the DFT level. The calculated relative equilibrium dissociation energies, ΔD_e, relative zero-point energy (ZPE) corrected dissociation energies, ΔD_0, molecular rotational constants, A, B, C, and electric dipole moment components, $\mu_{a,b,c}$ of the three most stable PFBA—FA conformers at the B3LYP-D3BJ and MP2/6-311++G(2d,p) levels are given in Table 1. The energies and spectroscopic parameters of the three higher energy conformers are given in Table 3. The structures of the three lowest energy conformers are shown in Fig. 18, while those of the next three higher energy ones are given in Fig. 23. The conformers are named as PFBA—FA-I to PFBA—FA-VI in decreasing order of stability, and we also refer to them simply as I, II ... to IV. From Table 3, one can see that PFBA—FA-I is strongly favored, by ~23 kJ mol^{-1}, over the other possible conformers.

PFBA—FA-I is made of the most stable PFBA and FA monomeric subunits where the carboxyl groups take on an antiperiplanar arrangement for the H(or C)–C–O–H chain i.e., the Z–COOH arrangement, rather than a syn-periplanar arrangement (the E–COOH arrangement) [72]. This heterodimer contains two intermolecular H–bonds by forming a cyclic eight-membered ring between the carboxyl groups of PFBA and FA, like other FA acid containing dimers studied. In all the other predicted PFBA—FA conformers, the carboxyl groups in both the PFBA and FA subunits are in the higher energy Z–COOH arrangement.

Preliminary searches for rotational transitions of the PFBA—FA dimers were carried out using the chirped pulse FTMW spectrometer in the 8–10 GHz range. We focused on the most stable conformer predicted since the other conformers are significantly less stable and are not expected to be populated in detectable amounts under supersonic jet expansion conditions. According to the ab initio calculations, we expected strong a-type and weak b- and c-type rotational transitions for the most stable conformer. One set of transitions were tentatively assigned to this conformer in the broadband scan, based mainly on recognizable a-type transition

Parameter	**I**	**II**	**III**	**I**	**II**	**III**
	B3LYP-D3BJ/6-311++G(2d,p)			MP2/6-311++G(2d,p)		
ΔD_e	0.00	23.54	34.23	0.00	19.58	28.23
ΔD_0	0.00	22.69	32.74	-	-	-
A	1158.51	1206.71	851.92	1155.39	1204.94	846.32
B	257.98	228.39	322.14	259.61	229.53	328.66
C	252.91	224.31	276.39	255.14	225.69	280.68
$\|\mu_a\|$	2.40	4.41	1.94	2.39	4.25	1.76
$\|\mu_b\|$	0.28	0.94	2.52	0.26	0.91	2.20
$\|\mu_c\|$	0.33	0.05	0.67	0.33	0.03	0.59

Table 3: Calculated relative raw dissociation energies ΔD_e, ZPE corrected dissociation energies ΔD_0 (in kJ mol^{-1}), rotational constants A, B, C (in MHz), and electric dipole moment components $|\mu_a|$, $|\mu_b|$, and $|\mu_c|$ (in Debye) of the three lowest energy PFBA—FA dimers at the B3LYP-D3BJ and MP2/6-311++G(2d, p) levels of theory.

patterns. A small section of the broadband spectrum used for the assignment is depicted in Fig. 2, showing such a-type transition pattern.

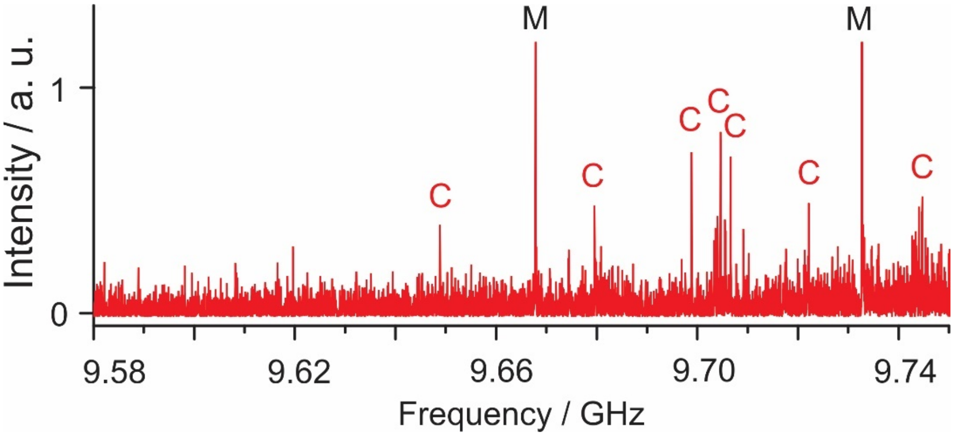

Figure 16: 0.27 GHz section of the broadband spectra measured with a sample PFBA+FA in helium. M indicates the rotational transitions of the PFBA monomer. C indicates the rotational transitions due to PFBA—FA-I, which are a-type, J=19←18 transitions.

The final frequency measurements were done with the cavity instrument and the

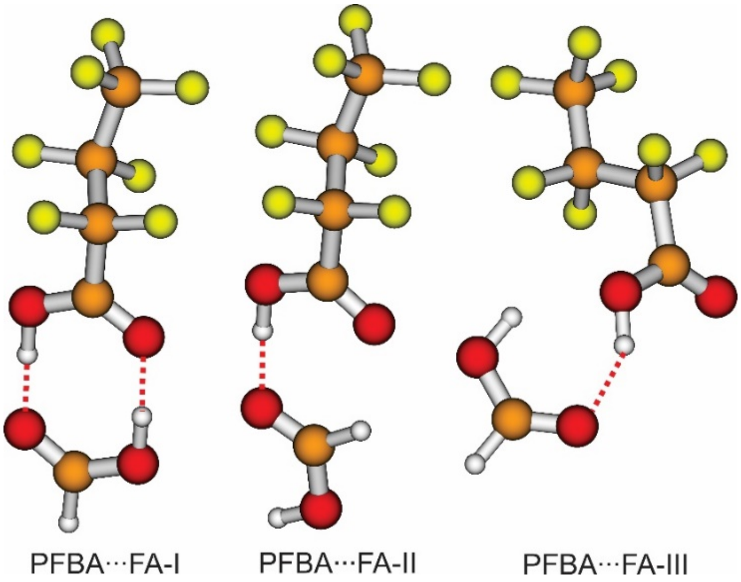

Figure 15: Optimized geometries of the three most stable conformers of PFBA—FA at the B3LYP-D3BJ/6-311++G(2d,p) level of theory.

measured frequencies were used in a fit with the PGOPHER program [73] utilizing Watson's Sreduction [74] Hamiltonian in its Irreducible representation. The resulting rotational and quartic centrifugal distortion constants are summarized in Table 4. All measured transition frequencies are summarized in Table S2, Supporting Information. Strong a-type and weak b- and c-type transitions were observed for the assigned dimer, in agreement with the ab initio calculated dipole moment components for PFBA—FA-I. The calculated rotational constants for PFBA—FA-I are in good agreement with the experimental data. The maximum deviation between calculated and experimental rotational constants is only 0.3% for the B3LYP-D3BJ calculation and 0.9% for the MP2 calculation. This indicates that the actual structure of the complex is very close to the B3LYP-D3BJ calculated one (Fig. 2). We note that in a number of H-bonded complexes, the B3LYP-D3BY calculations seem to provide consistently better agreement of rotational constants to the experimental ones than the MP2 calculations [43,44][75].

Parameters	PFBA—FA-I
A (MHz)	1161.38375(27)
B (MHz)	257.89494(22)
C (MHz)	252.79090(21)
D_J (kHz)	0.00943(10)
D_{JK} (kHz)	-0.04188(50)
D_K (kHz)	0.4816(73)
d_1 (kHz)	0.00080(18)
d_2 (kHz)	-0.000199(36)
N^a	78
σ (kHz)	1.9

Table 4: Experimental spectroscopic constants of PFBA—FA-I. ^{a} N is the number of rotational transitions included in the fit and σ is the standard deviation of the fit.

Unlike in the case of perfluoropropionic acid—FA [58], no splittings were detected in any of the rotational transitions of the PFBA—FA complex using the high-resolution cavity-based spectrometer. This indicates that the double proton transfer is quenched in the hetero acid dimer. In PFBA—FA-I, the double proton transfer requires a simultaneous heavy atom motion to convert PFBA into its mirror image to reach an equivalent potential energy minimum. In the case of the PFBA monomer, the barriers for the two possible conversion paths (as seen in Fig. 3 of Ref. [7]) from PFBA to its mirror image were calculated to be about 7.1 kJ mol^{-1} and 4.5 kJ mol^{-1}, respectively. We note that no tunneling splitting was detected for the PFBA monomer presumably because of the involvement of the heavy atoms in these motions. The second most stable conformer of the PFBA monomer is only supported by a very shallow well. In geometry optimizations of the acid dimer, a starting geometry with FA double H-bonding to the second most stable. PFBA conformer always converged to the PFBA—FA-I conformer. This suggests that double H-bonding with FA destabilizes the second PFBA conformer. Single H-bonding to the second PFBA conformer results in PFBA—FA-III (Fig. 18), which is significantly less stable than PFBA—FA-I (see Table 3). Overall, the conversion from the most stable PFBA configuration to its mirror image becomes even more difficult in the hetero acid dimer than in the monomeric form. The absence of double proton transfer splittings in the experimental spectra is consistent with the above discussion.

To obtain more insight into the non-covalent intermolecular interactions in this acid dimer, we carried out analyses using the Bader's Quantum Theory of Atoms in Molecules (QTAIM) [76,77] approach and the Non-Covalent Interactions [78] (NCI) method. Both approaches are implemented in the Multiwfn [79] program. The results of the QTAIM analysis is provided in Fig.20, where the presence of two intermolecular H-bonds in the complex are identified, as expected. It is interesting to note that the analysis also identifies the existence of a F—F type I attractive interaction in the PFBA monomer part of the complex.

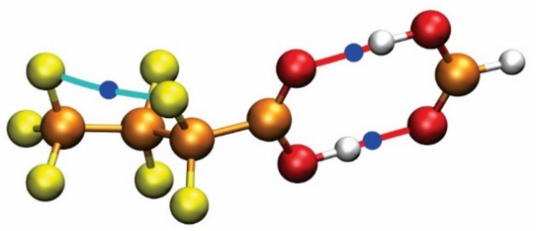

Figure 17: QTAIM analysis of PFBA—FA-I. Three bond critical points are identified. These are represented by blue dots. The bond paths through the bond critical points for the OH—O H-bonds and the F—F contact are shown in red and aqua colors.

NCI analysis is commonly used to visualize the non-covalent interactions, based on the electron density and its derivatives. In the NCI plots, the attractive and repulsive interactions are represented by isosurfaces with the color codes provided in Figure 21. We note that all QTAIM bond critical points have the corresponding attractive regions in the NCI analysis. One also gains some further insight into the intermolecular interactions in the acid dimer with the NCI plots. For example, the NCI plots show that the two intermolecular H-bonds in the PFBA—FA-I complex are not identical, i.e. one is stronger than the other. Indeed, the bond length of the (PFBA) C=O—HO (FA) H-bond is 1.68 Å, where the (PFBA) OH—O=C (FA) H-bond length is 1.58 Å. Because of this noticeable asymmetry in the H-bond lengths, the double proton transfer motion alone would result in a geometry which is none-equivalent to the current one if the PFBA subunit were to remain in the same position. The absence of the double proton tunneling in the PFBA—FA complex is therefore expected.

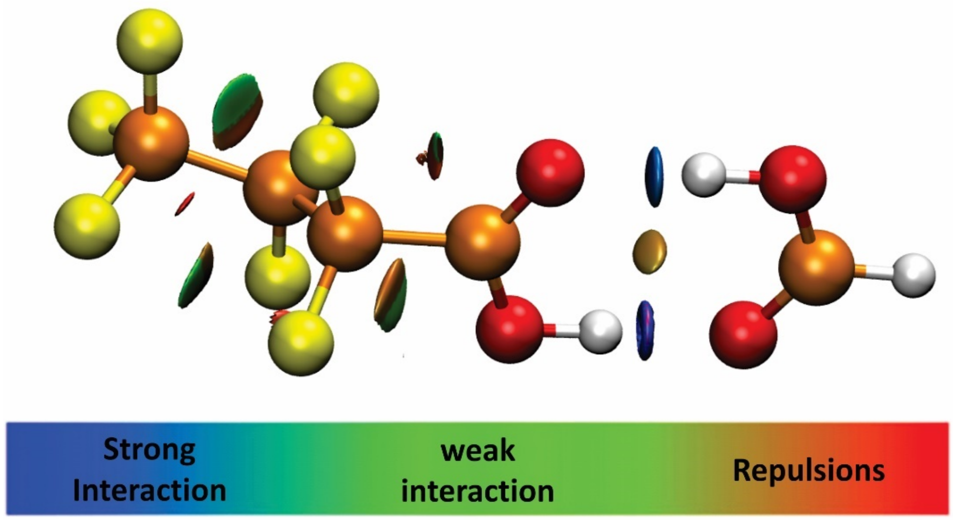

Figure 18: NCI plots of PFBA—FA-I. Blue and green colors indicate the presence of strong and weak attractive interactions, respectively, and the red and brown colors signify repulsive interactions.

Conclusions

The PFBA—FA complex was studied using rotational spectroscopy and high-level ab initio calculations. Conformational searches at the B3LYP-D3BJ and MP2 levels of theory identified the same six possible conformers with the lowest energy one being more stable by at least 22 kJ mol^{-1} than the others. This is consistent with the experimental detection of one single conformer. The experimental rotational constants are in excellent agreement with those from B3LYP-D3BJ calculations, indicating that the actual geometry is very similar to the ab initio structure. The non-covalent interactions present in the acid dimer were analyzed using the QTAIM and NCI methods. The latter shows that the two intermolecular H-bonds present are not identical, leading to the absence tunneling splitting in the observed rotational transitions. Both QTAIM and NCI analyses demonstrate the presence of attractive F—F interaction in the complex.

Supplemental

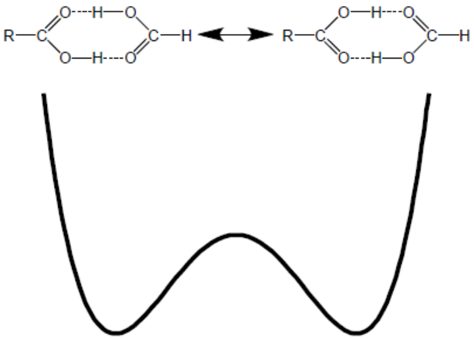

Figure 19: Double-minimum potential for a double proton transfer in planar molecules is presented. The two planar structures shown above are equivalent.

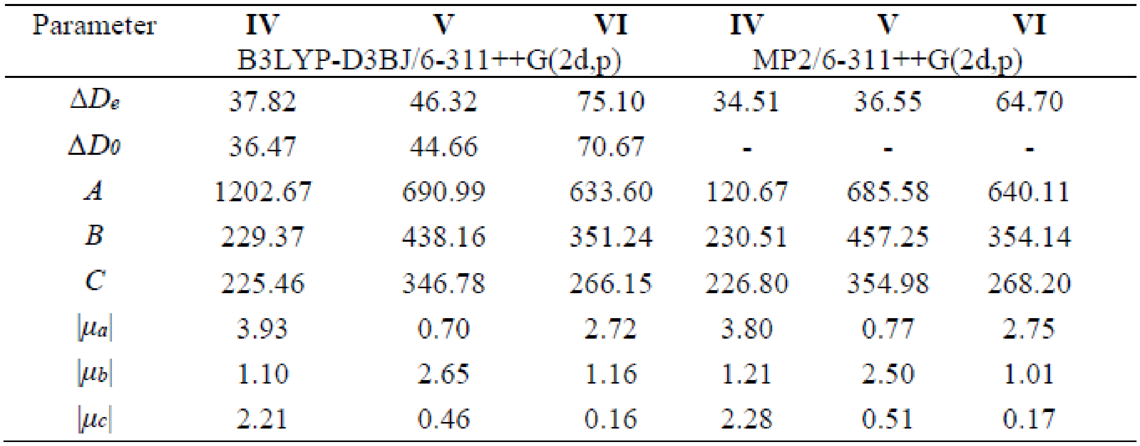

Parameter	IV	V	VI	IV	V	VI
	B3LYP-D3BJ/6-311++G(2d,p)			MP2/6-311++G(2d,p)		
ΔD_e	37.82	46.32	75.10	34.51	36.55	64.70
ΔD_0	36.47	44.66	70.67	-	-	-
A	1202.67	690.99	633.60	120.67	685.58	640.11
B	229.37	438.16	351.24	230.51	457.25	354.14
C	225.46	346.78	266.15	226.80	354.98	268.20
$\|\mu_a\|$	3.93	0.70	2.72	3.80	0.77	2.75
$\|\mu_b\|$	1.10	2.65	1.16	1.21	2.50	1.01
$\|\mu_c\|$	2.21	0.46	0.16	2.28	0.51	0.17

Table 5: Calculated relative raw dissociation energies ΔD_e, ZPE corrected dissociation energies ΔD_0 (in kJ mol-1), rotational constants A, B, C (in MHz), and electric dipole moment components $|\mu_a|$, $|\mu_b|$, and $|\mu_c|$ (in Debye) of the next three less stable PFBA—FA conformers at the B3LYP-D3BJ and MP2/6-311++G(2d,p) levels of theory.

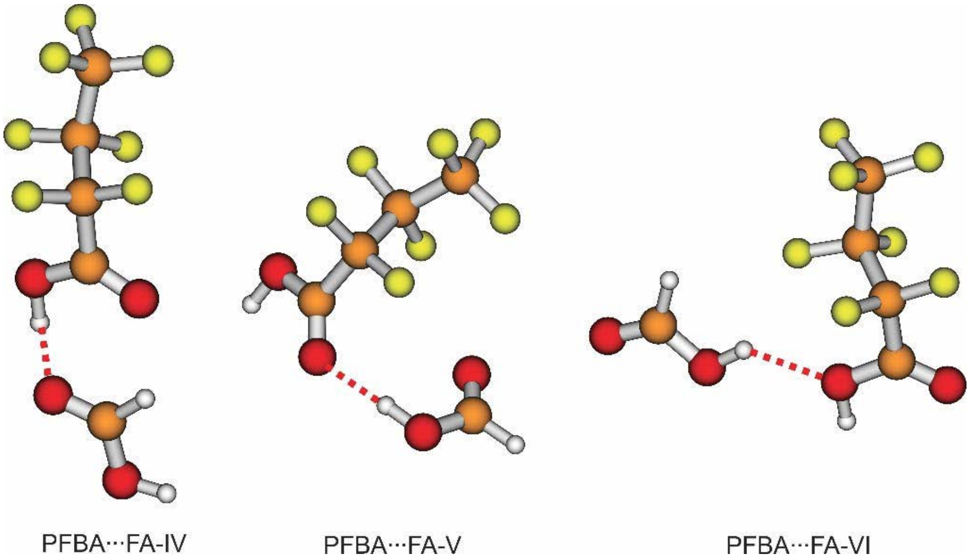

Figure 20 Optimized structures of the next three less stable conformers of PFBA—FA at the B3LYP-D3BJ/6-311++G(2d,p) level of theory.

J’	K_a’	K_c’	J’’	K_a’”	K_c’’	ν_{EXP} / MHz	$\Delta\nu^a$ / MHz
5	5	1	4	4	1	10707.6364	6E-4
5	5	0	4	4	0	10707.6364	6E-4
5	5	0	4	4	1	10707.6364	6E-4
5	5	1	4	4	0	10707.6364	6E-4
6	4	3	5	3	3	9406.333	-4E-4
6	4	2	5	3	2	9406.333	0.0012
6	4	2	5	3	3	9406.333	-4E-4
6	4	3	5	3	2	9406.333	0.0012
6	5	2	5	4	2	11218.3298	-2E-4
6	5	1	5	4	1	11218.3218	-0.0082
6	5	1	5	4	2	11218.3298	-2E-4
6	5	2	5	4	1	11218.3298	-2E-4
7	4	4	6	3	4	9917.0093	-3E-4
7	4	3	6	3	3	9917.0093	0.0044
7	4	3	6	3	4	9917.0093	-4E-4
7	4	4	6	3	3	9917.0093	0.0044
7	5	3	6	4	3	11729.0225	0.0016
7	5	2	6	4	2	11729.0225	0.0016
7	5	2	6	4	3	11729.0225	0.0016
7	5	3	6	4	2	11729.0225	0.0016
8	4	5	7	3	5	10427.6655	-0.0048
8	4	4	7	3	5	10427.6655	-0.0049
16	1	15	15	1	14	8207.7959	0.0018
16	2	14	15	2	13	8182.7208	0.001
16	3	13	15	3	12	8172.977	0
16	3	14	15	3	13	8172.4929	0.0011

16	4	12	15	4	11	8171.8805	-0.0032
16	5	11	15	5	10	8171.5244	3E-4
16	5	12	15	5	11	8171.5244	4E-4
16	6	10	15	6	9	8171.3458	0
16	6	11	15	6	10	8171.3458	0
16	7	9	15	7	8	8171.2482	-0.0011
16	7	10	15	7	9	8171.2482	-0.0011
16	2	15	15	2	14	8168.4618	-2E-4
16	0	16	15	0	15	8156.5485	-3E-4
16	1	16	15	1	15	8126.5898	0.0012
17	2	15	16	2	14	8695.6193	6E-4
17	1	16	16	1	15	8720.1828	-0.0012
17	3	14	16	3	13	8684.0922	-2E-4
17	3	15	16	3	14	8683.4347	1E-4
17	4	13	16	4	12	8682.7374	-0.0041
17	5	12	16	5	11	8682.308	7E-4
17	5	13	16	5	12	8682.308	8E-4
17	6	11	16	6	10	8682.0935	0.002
17	6	12	16	6	11	8682.0935	0.002
17	7	10	16	7	9	8681.9731	-2E-4
17	7	11	16	7	10	8681.9731	-2E-4
17	2	16	16	2	15	8678.6355	4E-4
17	0	17	16	0	16	8664.4744	0.0011
17	1	17	16	1	16	8634.0422	3E-4
18	2	16	17	2	15	9208.7362	-0.0017
18	3	15	17	3	14	9195.2738	1E-4
18	3	16	17	3	15	9194.3972	-5E-4
18	4	14	17	4	13	9193.6238	0.003
18	4	15	17	4	14	9193.6061	-3E-4
18	1	17	17	1	16	9232.4546	-2E-4
18	5	13	17	5	12	9193.1021	0
18	5	14	17	5	13	9193.1021	2E-4
18	7	11	17	7	10	9192.7007	-3E-4
18	7	12	17	7	11	9192.7007	-3E-4
18	6	12	17	6	11	9192.8437	-1E-4
18	6	13	17	6	12	9192.8437	-1E-4
18	2	17	17	2	16	9188.744	2E-4
18	0	18	17	0	17	9172.1084	8E-4
18	1	18	17	1	17	9141.4188	-0.0022
19	0	19	18	0	18	9679.4514	-0.0015
19	1	19	18	1	18	9648.7245	5E-4
19	2	18	18	2	17	9698.7831	-0.0013
19	1	18	18	1	17	9744.5958	-7E-4
19	2	17	18	2	16	9722.0714	-6E-4
19	3	16	18	3	15	9706.5272	-4E-4
19	4	16	18	4	15	9704.5005	-0.0015

19	4	15	18	4	14	9704.5297	0.0066
19	3	17	18	3	16	9705.3796	-1E-4
19	5	14	18	5	13	9703.9088	-2E-4
19	5	15	18	5	14	9703.9088	0
19	6	13	18	6	12	9703.6027	-4E-4
19	6	14	18	6	13	9703.6027	-4E-4

Table 6: Observed transition frequencies of the PFBA—FA-I dimer. [a] $\Delta\nu = \nu_{CALC}$.- ν_{EXP}.

CHAPTER V

CONFORMATIONAL ANALYSIS OF 3,3,3-TRIFLUORO-2-(TRIFLUOROMETHYL)PROPANOIC ACID

Introduction

Poly- and perfluorinated compounds are widely used for many industrial purposes [43]. In recent years, an increasing number of concerns have been raised regarding the contamination of ground-water by these compounds. For example, perfluorooctanoic acid (PFOA) – a man-made perfluorinated carboxylic acid (PFCA) that is a precursor to prevalent consumer goods, including polytetrafluoroethylene (commercially known as Teflon) – has been classified by the United States Environmental Protection Agency (EPA) as an “emerging contaminant”. On May 19, 2016, the EPA established a lifetime health advisory limit of 70 parts per trillion of PFOA in drinking water, based on the agency’s assessment of the latest peer-reviewed reports [6]. It is not surprising that major manufacturers, including DuPont, decided to phase out the use of PFOA, and some are looking to shorter chain PFCAs as replacements [45]. Similar to PFOA, these alternative PFCAs have both hydrophobic (alkyl fluoride) and hydrophilic (carboxylic acid) groups and are easily dissolved in water. Studies of the structures and dynamics of poly- and perfluorinated carboxylic acids in the gas phase can contribute to our understanding of the fates and impacts of these compounds in the aquatic environment.

Microwave (MW) spectroscopy is known to be a suitable technique for the investigation of the structures and dynamics of small molecules and their complexes in the gas phase [64,65].

Several short- chain PFCAs and their hydrates have been studied using microwave spectroscopy complemented by computational quantum chemistry, including trifluoroacetic acid [80], perfluoropropanoic acid [46,81], perfluorobutyric acid [7], and perfluoropentanoic acid [82]. For each of these short-chain PFCAs, only one dominant conformer, with the hydroxyl group roughly bisecting the F-C-C (alkyl fluoride) angle, was detected experimentally. It appears that repulsion between the hydroxyl group and the fluorine atoms is the dominant factor dictating the conformational preference. How are the conformational landscapes of fluorinated carboxylic acids affected by alkyl branching and/or only partial fluorination? Lin et al. recently investigated 2,3,3,3-tetrafluoropropanoic acid and found that the conformational landscape of this partially fluorinated molecule is more complicated than that of its perfluorinated counterpart [83]. The potential energy surfaces of partially fluorinated carboxylic acids tend to support multiple low energy conformers [84], and this feature may play an important role in their interactions with water and their reaction pathways in solution. On the other hand, we note that in a recent MW study of 3,3,3-trifluoropropanoic acid [85], only one conformer was detected experimentally.

In this paper, we report a combined MW spectroscopic and ab initio study of a representative branched polyfluorinated carboxylic acid, 3,3,3-trifluoro-2-(trifluoromethyl)propanoic acid (TTPA). The MW experiments were carried out at the University of Alberta using both chirped-pulse [69,70] and cavity-based [71] Fourier-transform MW (FTMW) spectrometers. Recently, these instruments have also been used in rotational spectroscopic studies of hydrogen-bonded systems, such as the methyl lactate-ammonia adduct [86]and the glycidol-propylene oxide complex [87]. The experimental work was complemented by high-level quantum chemistry calculations, from which multiple low energy conformers were located. Using this approach, we identified the most stable conformers of TTPA experimentally and obtained the related energetic information. To the best of the authors' knowledge, this is the first high-resolution spectroscopic study of gaseous TTPA.

Experimental

Survey scans were recorded using a chirped-pulse FTMW spectrometer [69,70], which is similar in design to those described earlier [88,89]. In short, a radiofrequency (rf) chirped pulse (0.2–1 GHz, 4 ls), generated by an arbitrary waveform generator (Tektronix, AWG 710B), is mixed with the output of a MW synthesizer to produce a 2 GHz MW chirp in the 8–18 GHz range. This chirped pulse is amplified using a 20W solid state MW amplifier (MW Power Inc., L0818-43) and then propagated into free space using a wide-band, high-gain MW horn antenna (rf/MW instrumentation, ATH7G18). The interaction of this chirped pulse with the molecular sample results in a free induction decay, which is received by a second horn antenna, recorded with a fast digital oscilloscope, averaged, and then Fourier-transformed to give the frequency spectrum. The spectral resolution of the broadband instrument is 25 kHz. All final frequency measurements were done with a cavity-based [37,90] pulsed-jet FTMW spectrometer, which has been described in detail elsewhere [71]. In this case, the frequency uncertainty is about 2 kHz. For the broadband survey scans, the sample mixture consisted of a trace amount of TTPA in 3 bar helium; for the final cavity-based measurements, it consisted of a trace amount of TTPA in 2 bar neon. TTPA (97%, Sigma Aldrich) was used without further purification and placed inside the nozzle cap. The TTPA sample was initially heated to 48°C in the chirped- pulse instrument, in order to increase the vapor pressure. However, this heating resulted in little signal enhancement, so the sample was not heated during the experiments using the cavity-based instrument.

Theoretical

Quantum chemistry calculations were performed using the Gaussian 09 program package [2] at the second-order Møller–Plesset perturbation theory (MP2) [91] and density functional theory (DFT) levels to determine the conformational landscape, structural parameters, and energetic information of the TTPA monomer. The Becke three-parameter Lee-Yang-Parr exchange-correlation (B3LYP) functional [92]was implemented with the 6-311G basis set [93] to scan the dihedral angle τ(O12-C5-C2-C1) (see Fig. 24 for atom labels) and to carry out further preliminary conformational searches, such as rotating the hydroxyl hydrogen atom toward the fluorine atoms. The resulting conformers were then re-optimized at the B3LYP/aug-cc-pVTZ level and, finally, at the MP2/aug-cc-pVTZ level. The structural and energetic information obtained from the calculations was used to aid in the MW spectroscopic investigation of these possible conformers.

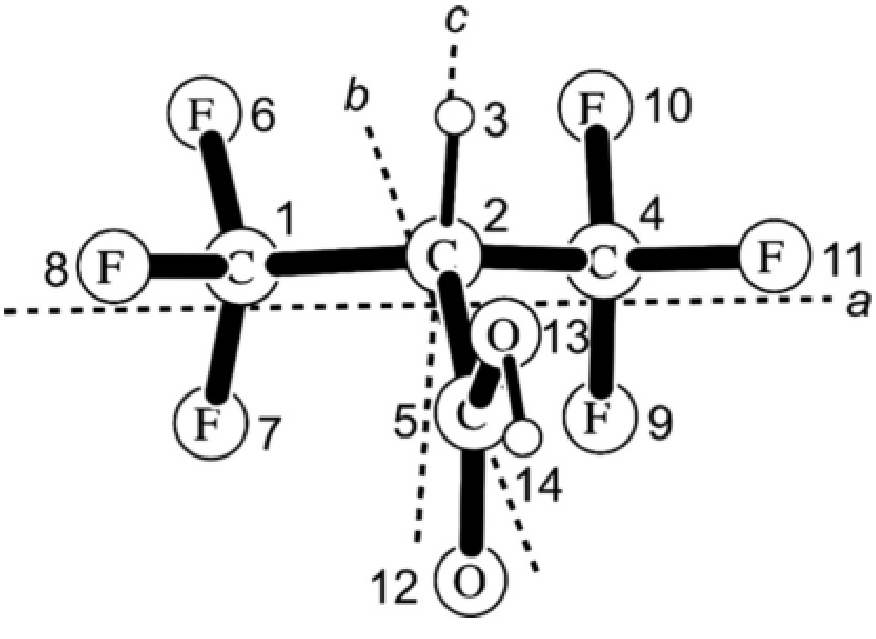

Figure 21: Atom labelling of 3,3,3-trifluoro-2-(trifluoromethyl)propanoic acid

Results and discussion

The potential energy scan along the dihedral angle $\tau(O_{12}\text{-}C_5\text{-}C_2\text{-}C_1)$ is shown in Fig. 25. The two most stable conformers of TTPA were identified in the scan. The carboxylic acid group of each conformer is in its Z orientation, in which the C-R bond is in the trans arrangement to the hydroxyl group. In this paper, we refer to the conformers in which $\tau(O_{12}\text{-}C_5\text{-}C_2\text{-}C_1)$ is approximately 63° and ~115° as TTPA-I and -II, respectively. After zero-point-energy correction, TTPA-I is approximately 0.4 kJ/mol more stable than TTPA-II, so both might be expected to be observable experimentally. We also considered two additional conformers, which feature the carboxylic acid group in its E orientation, with the acidic hydrogen atom oriented toward the fluorine atoms. We refer to the two additional conformers as TTPA - III and - IV, in decreasing order of stability, based on ΔD_0. TTPA-III and -IV are about 14 and 23 kJ/mol less stable than TTPA-I, respectively, and might be difficult to detect in the jet expansion. All four conformers identified computationally are shown in Fig. 3, and the predicted energetic information and spectroscopic constants are provided in Table 1. The initial broadband rotational scan of TTPA in helium was recorded in the 8–10 GHz frequency region. An observed set of strong transitions could be assigned by comparison to the spectrum simulated in the program PGOPHER, using the theoretical rotational constants of TTPA-I [73]. The next conformer, TTPA-II, was identified in a similar fashion. Both conformers exhibit only b- and c-type transitions; due to symmetry about the bc plane, $\mu_a = 0$ D for each. Indeed, the experimental relative intensities of the b- and c-type transitions in the broadband spectra of TTPA-I and -II are in good agreement with the ab initio predicted intensities. A total of 37 and 36 transitions were measured for TTPA-I and -II, respectively, using the cavity-based spectrometer.

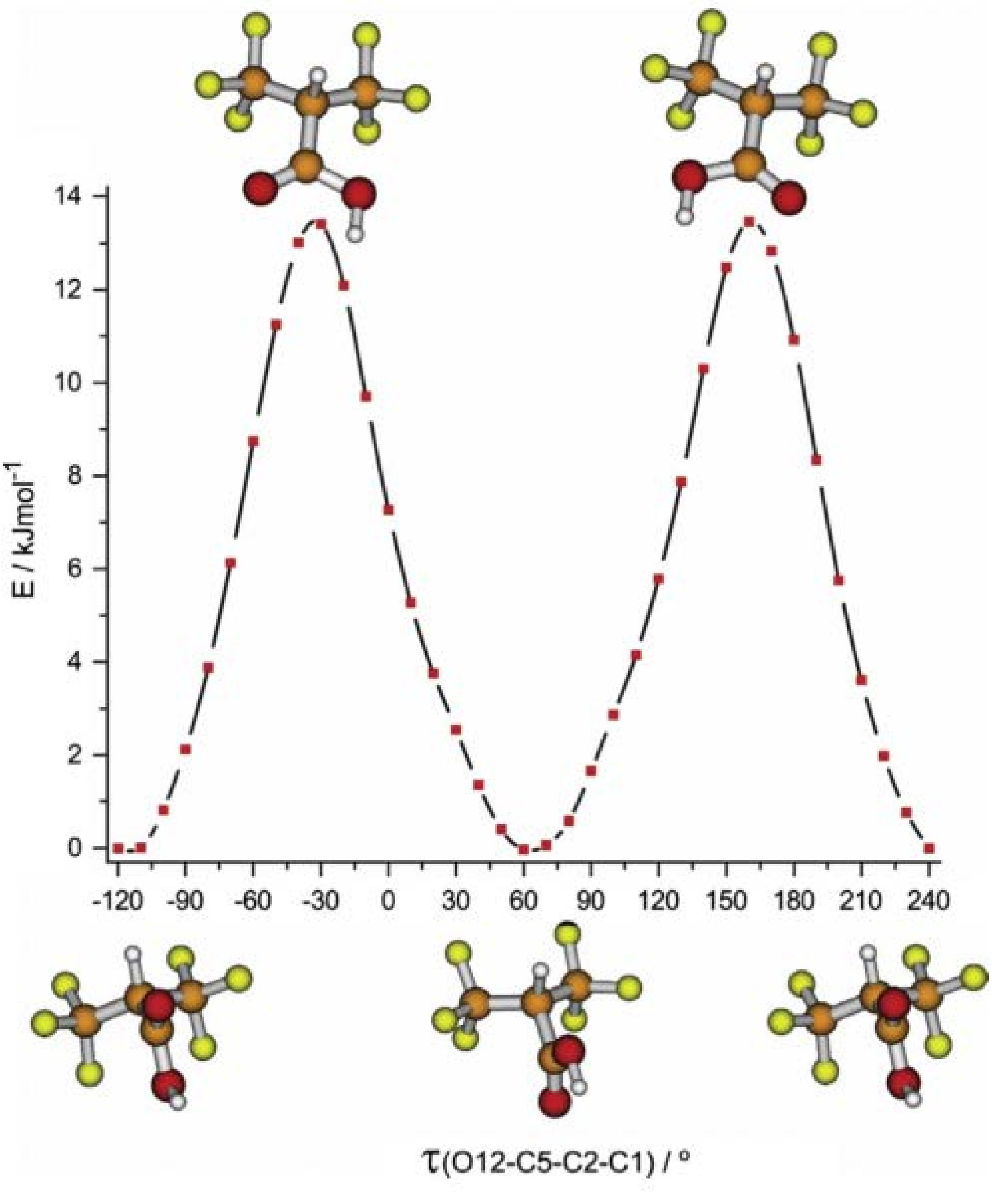

Figure 22: Potential energy scan along the dihedral angle τ(O12-C5-C2-C1) in steps of 10°. The calculations were done at the B3LYP/6-311G level.

These transitions were fit to Watson’s A-reduction Hamiltonian in its irreducible representation [94], using the SPFIT program developed by Pickett [3]. The standard deviations of the fits – about 3 and 2 kHz for TTPA-I and -II, respectively – are on the same order as the experimental uncertainty. The measured transition frequencies, their assignments, and the differences from the calculated frequencies are provided in the Table 9 and 10. The fitted rotational constants and centrifugal distortion constants are summarized in Table 7. It is interesting to compare the experimental rotational constants with those calculated at the DFT and MP2 levels. The differences between the predicted rotational constants of the two most stable conformers at a given level of theory are comparable to the differences between the predicted rotational constants of a given conformer at the two levels of theory, potentially complicating the assignments. For example, it would be questionable to assign the spectrum of the most stable observed conformer to TTPA-I based upon comparison to only the DFT rotational constants, because the observed rotational constants are actually in better agreement with the predicted rotational constants of TTPA-II at the DFT level. In contrast, the fitted ground-state rotational constants of both observed conformers agree very well with the respective calculated

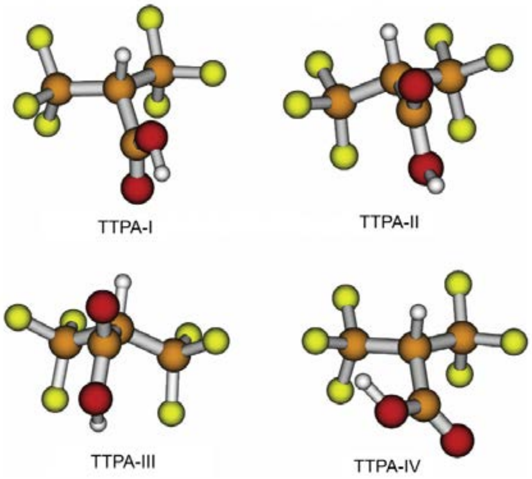

Figure 23: Geometries of the four TTPA conformers identified computationally

Parameter[a]	TTPA I	TTPA II
A (MHz)	1075.53107(56)	1085.63313(37)
B (MHz)	975.17899(41)	975.16102(34)
C (MHz)	688.28340(34)	692.86057(21)
D_{J} (kHz)	0.0359(73)	0.0396(60)
$D_{J\mathrm{K}}$ (kHz)	0.730(31)	0.402(23)
D_{K} (kHz)	-0.724(21)	-0.394 (16)
d_J (kHz)	0.0114(26)	0.0131(27)
d_{K} (kHz)	0.029(10)	-0.0385(79)
N	37	36
σ (kHz)	2.8	1.7

Table 7: Experimental spectroscopic constants of two conformers of TTPA

equilibrium rotational constants at the MP2 level. We also note that the predicted rotational constants of TTPA-II and -III are also very similar, because the main difference in their structures is the orientation of the hydrogen atom of the hydroxyl group. However, the l_b/l_c ratio differs greatly from one conformer to the other. Indeed, the intensity ratios of the assigned b- and c-type transitions allow unambiguous conformational identifications.

A comparison of the preferred geometries and energetics of the conformers of TTPA with those of related poly- and perfluorinated carboxylic acids previously studied using rotational spectroscopy provides further insight. Like many other fluorinated alkyl carboxylic acids investigated to date, TTPA in its most stable configuration, i.e. TTPA-I, adopts the Z orientation of the carboxylic acid group. The general preference for the Z form was attributed initially to intramolecular C=OH···O hydrogen bonding and later to hyperconjugative effects [95,96]. In recent years, quantum chemistry calculations have shown that hyperconjugative interactions are not responsible for this preference. The most important energy term for the Z preference comes from electrostatic interactions. Specifically, the attraction of the electron density of the carbonyl oxygen by the nucleus of the acidic hydrogen [97–99]. In a quantum theory of atoms in molecules (QTAIM) [100]analysis of TTPA, no bond critical point (BCP) was located between the carbonyl oxygen atom and the acidic hydrogen atom (see Fig. 23, Supporting Information); this absence suggests that there is no intramolecular C=O···HO hydrogen bond in the carboxylic acid group of either of the two TTPA conformers observed. A QTAIM analysis of formic acid has led to the same conclusion [99].

	TTPA I			TTPA II			TTPA III		TTPA IV	
Parameters	B3LYP/ aug-cc-pVTZ	MP2/Aug -cc-pVTZ	Exp.	B3LYP/ aug-cc-pVTZ	MP2/Aug -cc-pVTZ	Exp.	B3LYP/ aug-cc-pVTZ	MP2/Aug -cc-pVTZ	B3LYP/ aug-cc-pVTZ	MP2/Aug -cc-pVTZ
ΔD(kJ/mol)				0.48	0.42		14.3	13.9	23.5	23.0
A/(MHz)	1063.6	1078.1	1075.5	1073.5	1087.8	1085.6	1074	1088	1129.1	1148
B/(MHz)	963	977.1	975.2	962.7	977.2	975.2	965.4	980	952.6	967.4
C/(MHz)	680.5	692.6	688.3	684.9	696.6	692.9	688.1	699.3	656.9	671

Table 8: Calculated relative well depths, relative dissociation energies, rotational constants, and dipole moment components of the four TTPA conformers at the B3LYP/aug-cc- pVTZ and MP2/aug-cc-pVTZ levels.

Another structural feature of interest is the position of the carboxylic acid group along the fluorocarbon chain. Only one dominant conformer was detected for each of the following four short-chain PFCAs in a molecular jet expansion: CF_3COOH [101], CF_3CF_2COOH [46],$CF_3(CF_2)2COOH$ [7], and $CF_3(CF_2)_3COOH$ [82]. The most stable conformers feature very similar geometries, in which the hydroxyl group roughly bisects the F-C_{acid}-R angle in a Newman projection along the C_{acid}–C bond (for example, see Fig. 4 in Ref. [7][70]). The main driving force for the conformational preference in each of these acids is the minimization of the repulsion between the hydroxyl group and the fluorine atoms; repulsion between the carbonyl group and the fluorine atoms plays a secondary role. It appears that for TTPA, the same main driving force is at work. The shortest HO···F distances in TTPA-I and -II are 3.325 and 2.918 Å, respectively; the shortest C=O···F distances in TTPA-I and -II are 3.021 and 3.351 Å, respectively. TTPA can be seen as a derivative of CF_3CH_2COOH [85] where one hydrogen atom of CH_2 is substituted with a CF_3 group. Again, the only conformer of CF_3CH_2COOH observed experimentally favors the geometry in which the oxygen atom of the hydroxyl group is as far from the fluorine atoms as possible – even though the closest fluorine atoms are already much further from the hydroxyl group in CF_3CH_2COOH than in TTPA. This repulsive driving force also results in a conformational barrier between TTPA-II and TTPA-I (13.6 kJ/mol) that is much higher than the related barrier in CF_3CH_2COOH (about 1 kJ/mol). Another partially fluorinated carboxylic acid studied by MW spectroscopy is $CH_3CHFCOOH$ [102]. Interestingly, the two experimentally observed conformers are characterized by the Z and E forms of the carboxylic acid group, respectively. Because the fluorine atom is situated at the α-position, relative to the carboxylic acid group, it may participate in an intramolecular OH···F–C hydrogen-bond in the E form of the acid, accounting for the surprising stability of this conformer [38][102].

The results of QTAIM analyses of the two observed conformers of TTPA are shown in the molecular graphs in Fig. 23. A BCP is located between two of the fluorine atoms in TTPA-II, indicating the presence of a fluorine···fluorine close contact [103]. Noncovalent F···F interactions involving organofluorines have attracted much recent attention due to their importance in topics such as polymorphism and crystal engineering [104]. Short type-I and -II C–F···F–C close contacts have been observed in the crystal packing of compounds containing a perfluorinated chain, such as $CF_3(CF_2)_5CH_2CH(CH_3)$ COOH, $CF_3(CF_2)_5(CH_2)_4(CF_2)_5CF_3$ and $\{CF_3(CF_2)_5CH_2CH_2\}_3P{=}O$ [105]. Type-I close contacts can be regarded as van der Waals interactions when two F atoms interface the neutral regions of their electrostatic potential surfaces and minimize repulsion. Type-II contacts, on the other hand, occur when the electrophilic region of one F atom interacts with the nucleophilic region of another F atom, leading to an L-shaped geometry [103]. Quantum chemistry calculations were performed on the corresponding dimers in conformations that are consistent with the crystal packing. The existence of F···F bonds in each of these dimers was confirmed by the presence of BCPs using QTAIM analyses [105]

It has been reported that higher-lying E conformers of a number of carboxylic acids [106], such as para-substituted benzoic acid derivatives [107] and oxalic acid, [108] prepared in low- temperature matrices can convert to lower-lying Z conformers through a tunneling process. The isomerization barrier is too high to be overcome at the low matrix temperatures. In the current work, the E forms of TTPA (i.e., TTPA-III and -IV) were not observed experimentally. This is consistent with the fact that the E forms are predicted to be much less stable than the Z forms (i.e., TTPA-I and -II) and are therefore barely populated in the jet expansion. Since the energy difference between the Z and E forms is so large, one does not expect to see any tunneling splittings due to the rotation of the hydroxyl group. No internal rotation splittings associated with the CF_3 rotors were observed either; similarly, no hyperfine splittings were reported for the other PFCAs studied previously [6,8,9,37][7,80,81,101].

Conclusions

The rotational spectrum of TTPA was measured for the first time using both chirped-pulse and cavity-based FTMW spectrometers. Two conformers were observed experimentally and identified unambiguously, each with the carboxylic acid group in its Z orientation. The rotational constants of the observed conformers are in excellent agreement with those from the quantum chemical structures, which feature a dihedral angles $\tau(O_{12}\text{-}C_5\text{-}C_2\text{-}C_1)$ of approximately 63^o and -115^o, respectively. Comparison of TTPA and previously reported fluorinated carboxylic acids shows some noticeable differences in their preferred geometries and conformational energetics, such as the interconversion barrier height between the conformers, highlighting the diversity of conformational landscapes in this class of compounds.

J'	Ka'	Kc'	J"	Ka"	Kc"	ν_{EXP} / MHz	$\Delta\nu^a$ / MHz
5	0	5	4	1	4	7216.0854	0.0011
5	1	5	4	0	5	7216.4870	0.0012
4	3	2	3	2	1	7494.3183	0.0060
5	3	2	4	2	3	7873.4914	-0.0013
5	2	4	4	1	3	7897.8757	-0.0004
4	2	2	3	1	2	8044.1480	-0.0031
4	3	1	3	2	1	8056.4588	0.0008
4	1	3	3	0	3	8148.4339	0.0022
4	2	3	3	1	3	8166.4928	0.0005
4	3	2	3	2	2	8220.1381	0.0006
4	4	1	3	3	0	8312.3210	-0.0010
5	2	3	4	3	2	8373.1647	-0.0029
4	4	0	3	3	0	8379.1722	-0.0016
4	4	1	3	3	1	8439.8031	-0.0020
4	4	0	3	3	1	8506.6527	-0.0042
6	0	6	5	1	5	8592.7499	-0.0016
6	1	6	5	0	5	8592.7957	0.0021
5	3	3	4	2	2	8732.9064	-0.0008
4	3	1	3	2	2	8782.2847	0.0015
6	3	3	5	2	4	9258.9293	0.0003
6	2	5	5	3	2	9262.5508	-0.0001
4	2	2	3	1	3	9638.0417	0.0040
5	4	2	4	3	1	9740.0870	0.0036
6	4	2	5	3	3	9889.6227	-0.0010
7	1	7	6	0	6	9969.2904	-0.0006
5	1	4	4	2	2	10019.6029	-0.0032
5	4	1	4	3	1	10131.3277	-0.0006
5	2	3	4	1	3	10145.8702	-0.0044
6	1	5	5	4	2	10184.6914	0.0037
5	3	2	4	0	4	10201.8311	-0.0006
5	4	2	4	3	2	10302.2267	-0.0023
5	5	1	4	4	0	10507.6203	-0.0013
5	5	0	4	4	0	10538.9866	-0.0019
5	5	1	4	4	1	10574.4715	-0.0018
5	5	0	4	4	1	10605.4715	0.0095
7	3	4	6	2	5	10636.4296	-0.0001
7	2	6	6	3	3	10636.8927	0.0002

Table 9 Observed transition frequencies of the TTPA-I conformer

J'	Ka'	Kc'	J"	Ka"	Kc"	ν_{EXP} / MHz	$\Delta\nu^a$ / MHz
5	0	5	4	1	4	7216.4689	0.0000
5	1	5	4	0	4	7262.0629	0.0000
4	3	3	3	2	1	7563.7648	0.0011
5	3	2	4	2	3	7914.7722	0.0010
5	2	4	4	1	3	7947.4247	-0.0044
4	2	2	3	1	2	8059.0068	0.0001
4	3	1	3	2	1	8089.0795	0.0008
4	2	3	3	1	3	8200.1081	0.0020
4	3	2	3	2	2	8264.1253	0.0013
5	2	3	4	3	2	8376.5726	0.0018
4	4	1	3	3	0	8391.8607	-0.0043
4	4	0	3	3	0	8448.8113	0.0010
4	4	1	3	3	1	8507.1326	0.0007
4	4	0	3	3	1	8564.0770	0.0000
6	0	6	5	1	5	8647.3606	-0.0006
6	1	6	5	0	5	8647.4294	-0.0002
4	3	1	3	2	2	8789.4367	-0.0021
5	3	3	4	2	2	8809.8282	0.0021
6	3	3	5	2	4	9312.3528	-0.0013
6	2	5	5	3	2	9317.7006	0.0000
5	4	2	4	3	1	9837.3878	0.0011
6	4	2	5	3	3	9929.3405	0.0013
7	2	5	6	1	6	10033.0559	-0.0021
7	1	7	6	0	6	10033.0694	0.0039
5	1	4	4	2	2	10040.2775	-0.0009
6	3	4	5	2	3	10055.7582	-0.0002
5	2	3	4	1	3	10171.2614	0.0005
5	4	1	4	3	1	10186.0197	-0.0011
5	3	3	4	2	3	10247.2573	-0.0023
5	4	2	4	3	2	10362.7035	0.0018
5	5	1	4	4	0	10605.3766	-0.0012
5	5	0	4	4	0	10630.5119	0.0004
5	5	1	4	4	1	10662.3246	0.0016
5	5	0	4	4	1	10687.4560	-0.0006
7	3	4	6	2	5	10699.5949	-0.0007
7	2	6	6	3	3	10700.3477	-0.0007

Table 10 Observed transition frequencies of the TTPA-II conformer.

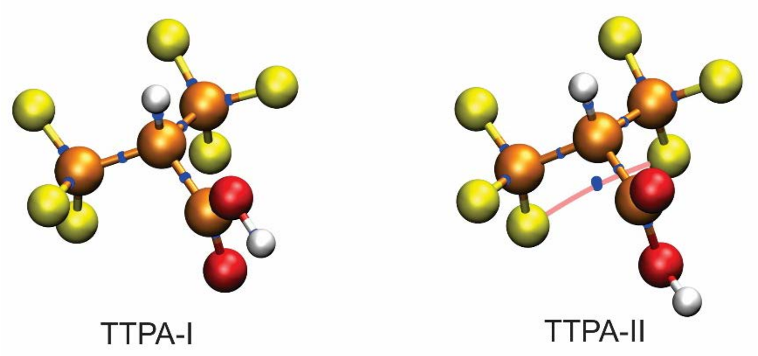

Figure 24 QTAIM analysis on the two TTPA conformers observed. Blue dots indicate the bond critical points identified. Please note that no bond critical points are identified for the potential C=O··HO intramolecular hydrogen bond in either conformers. A bond critical point is identified in TTPA-II, indicating the existence of a close F··F contact.

CHAPTER VI

MICROWAVE MEASUREMENTS OF THE TROPOLONE—FORMIC ACID DOUBLY HYDROGEN BONDED DIMER

Introduction

Proton tunneling is a large-amplitude vibrational motion which has been observed and could be present in a wide range of molecules and complexes involved in important chemical reactions and biological systems such as DNA. The tropolone monomer exhibits proton tunneling, and this work was initiated to look for possible proton tunneling in the tropolone–formic acid doubly hydrogen-bonded dimer.

Tropolone (2-hydroxy-2,4,6-cycloheptatrien-1-one), a seven-membered ring pseudoaromatic molecule, is considered as a prototypical molecule for proton transfer. The carbonyl group is located on one of the carbon atoms within the ring, and the OH group is attached to the carbon atom at the α position with respect to the carbonyl group. The neighboring C==O and OH groups interact and form an intramolecular hydrogen bond. The non-symmetric hydrogen atom tunnels between the two carbonyl oxygen atoms during the tautomerization of the carbon ring. The resulting structure after the tunneling motion is identical to the structure beforehand. This tunneling effect results in a double minimum well in the potential energy surface and a transition state of $C_{2V}(M)$ symmetry along the proton-transfer coordinates. The tunneling motion is described by a vibrational motion which results in two vibrational states that represent each of the tunneling states observed. This proton tunneling effect has been extensively studied using microwave spectroscopy,[55,56] rotationally resolved degenerate four-wave mixing, [109–113] matrix-isolated infrared spectroscopy, [114,115] laser-induced fluorescence (LIF) techniques,[116,117] and gaseous infrared spectroscopy.[118–121]

The magnitude of the tunneling splitting of tropolone can be affected by a number of factors. Among them are the motion of the tunneling proton, the displacement of heavy nuclei, redistribution of electronic charge density among various atoms, energy, and mode of vibrational excitation, and introduced asymmetric isotopic substitutions. The barrier height can also be influenced by intermolecular interactions, such as forming van der Waals complexes with rare gases or hydrogen bonded systems with other carboxylic acids. These intermolecular interactions can both perturb the molecule’s vibrational coupling and change the barrier height and shape of the potential energy surface. The rare gases Ar, Kr, and Xe were the simplest complexing agents studied to form the tropolone van der Waals complexes. Sekiya et al.[122] studied the fluorescence excitation spectra of jet-cooled tropolone-Rg (Rg = Ar, Kr, Xe). They found that the tunneling doublet separation $|\Delta_v^{'} - \Delta_0^{''}|$ for the tunneling states of Ar-tropolone to be close to that of the tropolone monomer. $\Delta_v^{'}$ is the tunneling splitting of the υ level in $\tilde{A}^1B_2$ state, and $\Delta_0^{''}$ is that of the zero-point level in $\tilde{\mathrm{X}}_1\mathrm{A}_1$. Lin et al.[123] reported the microwave spectrum of Ar-tropolone and found that even the weak interaction between argon and tropolone quenches the proton tunneling. Keske and Plusquellic[124] reported the microwave spectrum of tropolone-H2O and found that the tropolone monomer tunneling splitting vanishes upon addition of a water molecule.

Formic acid (FA) is known to form doubly hydrogen-bonded dimers with several carboxylic acids [10–16] that exhibit a concerted double proton tunneling. Some other doubly hydrogen-bonded dimers do not exhibit the concerted proton tunneling. [17,18] We recently reported the microwave spectrum of cyclopropanecarboxylic acid–formic acid (CPCA-FA) dimer [19] and no tunneling was observed for this doubly hydrogen-bonded dimer. The doubly hydrogen-bonded tropolone–formic acid dimer introduces a new interesting question about whether or not the tunneling splitting can be observed in this larger more symmetric complex. We expect the concerted double proton tunneling motion to be present in the dimer since it possesses the requiredC_{2v}(M) symmetry, but the tunneling splittings would not be observed if the potential barrier is too high. In this paper, we report the microwave spectrum and ab initio calculations of the tropolone–formic acid doubly hydrogen-bonded dimer.

Microwave measurements

The microwave spectrum was measured for the tropolone–formic acid doubly hydrogen-bonded dimer in the 4.7–9 GHz range, and all the assigned transitions are shown in Table I. These measurements were taken using a Flygare-Balle type pulsed-beam Fourier transform microwave spectrometer that has been previously described. [125,126]The tropolone (98%) and formic acid (98%) samples were both purchased from Sigma Aldrich and used without further purification. The samples were transferred to separate glass sample cells. The cell containing tropolone was placed in the Ne gas line just before the pulsed valve (General Valve, Series 9) and was set to pulse at room temperature. The Ne backing pressure was maintained at about 1 atm. The tropolone sample was pulsed until there was a strong parent test signal recorded. Once the tropolone signal was sufficiently strong, the sample cell containing the formic acid was placed in the Ne gas line, before the tropolone sample, and the formic acid vapor was passed over the tropolone sample with each molecular beam pulse. The sample of formic acid was brought to −8°C before attaching to the Ne gas line and this temperature was maintained using a

Peltier cooling device. The formic acid vapor was pulsed over the solid tropolone sample for about 15 min and then was removed from the Ne gas line as this provided a sufficient concentration of formic acid to measure the dimer transitions in a single pulsed beam cycle.

Calculations and rotational constants

Ab initio calculations were performed on the HPC (High-Performance Computing) system at the University of Arizona using the Gaussian 09 [127] using the B3LYP method with the aug-cc-pVTZ basis. The results from this calculation are shown in Table 9, and the calculated structure showing the hydrogen bond lengths is shown in Figure 27. The calculated rotational constants were used in the Pickett SPCAT [3] program to predict the rotational transitions expected to be observed. The calculated dipole moment components were 3.8 D along the a-axis and 0.6 D along the b-axis, so it was expected that the a-type transitions would be the strongest and these were the transitions that were initially searched for. The rotational and centrifugal distortion constants were determined from the measured 25 a- and b-type rotational transitions using the Pickett SPFIT program, and the experimentally determined parameters are also shown in Table 10

	Parent(experimental)	B3LYP/aug-cc-pVTZ
A/MHz	2180.7186(98)	2191.3931
B/MHz	470.87390(25)	474.39567
C/MHZ	387.68984(22)	389.97457
D_J/kHz	0.0100(14)	
D_{JK}/kHz	0.102(28)	
D_K/kHz	13.2(81)	
Δ/*amu Å2*	−1.46	-0.003
N	25	
σ/kHz	3	

Table 11 Experimentally determined parameters

$J'_{K_a' K_c'}$	$J''_{K_a'' K_c''}$	ν_{obs}	ν_{o-c}
$4_{1\,4}$	$3_{0\,3}$	4776.994	0.006
$6_{1\,6}$	$5_{1\,5}$	4879.911	-0.001
$6_{0\,6}$	$5_{0\,5}$	5051.614	-0.002
$6_{3\,3}$	$5_{3\,2}$	5169.534	0.000
$6_{2\,4}$	$5_{2\,3}$	5237.764	0.000
$5_{1\,5}$	$4_{0\,4}$	5444.692	-0.007
$7_{1\,7}$	$6_{1\,6}$	5683.893	0.004
$7_{0\,7}$	$6_{0\,6}$	5855.119	0.004
$7_{3\,5}$	$6_{3\,4}$	6030.552	0.001
$7_{3\,4}$	$6_{3\,3}$	6038.775	0.002
$6_{1\,6}$	$5_{0\,5}$	6089.936	0.003
$7_{2\,5}$	$6_{2\,4}$	6141.604	-0.005
$7_{1\,6}$	$6_{1\,5}$	6257.955	0.001
$8_{1\,8}$	$7_{1\,7}$	6484.354	0.001
$8_{0\,8}$	$7_{0\,7}$	6646.059	-0.001
$7_{1\,7}$	$6_{0\,6}$	6722.206	0.000
$8_{1\,7}$	$7_{1\,6}$	7133.512	0.003
$9_{1\,9}$	$8_{1\,8}$	7281.295	-0.003
$8_{1\,8}$	$7_{0\,7}$	7351.443	-0.001
$9_{0\,9}$	$8_{0\,8}$	7426.650	-0.002
$9_{1\,9}$	$8_{0\,8}$	7986.682	-0.001
$10_{0\,10}$	$9_{0\,9}$	8199.868	-0.003
$10_{1\,9}$	$9_{1\,8}$	8856.853	-0.003
$11_{1\,11}$	$10_{1\,10}$	8865.250	0.005
$11_{0\,11}$	$10_{0\,10}$	8968.743	0.000

Table 12 Measured a- and b-type rotational transitions of the tropolone–formic acid doubly hydrogen-bonded dimer. Values are shown in MHz.

Discussion

The rotational spectrum was measured for the tropolone–formic acid doubly hydrogen-bonded dimer in the 4.7-9 GHz range using a pulsed-beam Fourier transform microwave spectrometer. It was expected that this doubly hydrogen-bonded dimer would exhibit a concerted double proton tunneling motion as the dimer has a C_{2v}(M) symmetry. This symmetry has been proposed as a requirement to observe the proton tunneling motion, and this symmetry has been present in numerous other hydrogen-bonded dimers exhibiting observable tunneling splittings.

When the doubly hydrogen-bonded dimer exhibits proton tunneling, each rotational transition measured is split; the magnitude of this splitting ranges up to a few MHz for a-type transitions and it can be hundreds of MHz for b-type transitions and is dependent on the barrier height and separation of the minima for the potential energy surface. When the splittings due to tunneling are observed, a vibration-rotation coupling analysis needs to be performed to fit the spectra from the two tunneling states which are treated as two vibrational states. After measuring both a- and b-type transitions for this dimer, no splittings for any transition were observed indicating that this doubly hydrogen-bonded dimer did not exhibit the concerted double proton tunneling motion.

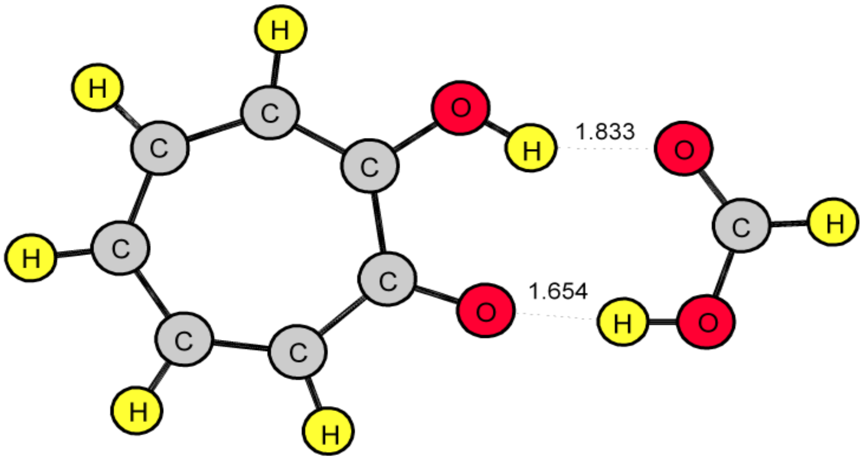

Figure 25: Calculated B3LYP/aug-cc-pVTZ structure of the Tropolone–Formic Acid doubly hydrogen-bonded dimer. Hydrogen bond lengths are shown in Å.

To get an estimate of the barrier height in the potential energy surface for the tunneling motion, the two tunneling protons were held fixed between the tropolone and formic acid molecules such that the distance of the proton between the two oxygen atoms in each molecule was equivalent, and the energy of this transition-state structure was calculated using B3LYP/aug-cc-pVTZ. The difference in energy of the calculated equilibrium structure and this transition state structure was about 15 000 cm^{-1}. The distance that each proton was estimated to move during the tunneling process is about 0.8 Å, which is similar to what was found for the propiolic–formic acid dimer.[11,12] The distance each proton moves was found by taking the transition state O—H bond lengths and subtracting the B3LYP optimized bond lengths and multiplying by 2 to get to the next tunneling state. The large barrier height between the two tunneling states is, very likely, why the concerted double proton tunneling motion was not observed for this doubly hydrogen-bonded dimer. The estimated distance between the potential minima was similar to that for propiolic acid–formic acid complex for which the proton tunneling process was observed in the microwave spectra.

While measuring the rotational transitions from this dimer, the spectrum was congested with numerous other transitions that were significantly strong. From the ab initio calculations, it was predicted that there are many low energy out of plane vibrational modes. The inertial defect calculated from the experimentally determined rotational constants is $\Delta = -1.46$ amu $Å^2$. This is indicative of a planar structure with the magnitude not being significantly large, but because of the nonzero negative value, this is a confirmation that there are significant out of plane vibrations for this dimer. [128] After measuring many transitions and attempting to make sense and assign the congested spectra, none of the additional transitions measured were able to be fit to an excited vibrational state. The additional transitions are most likely from other complexes formed with formic acid or water or due to the excited vibrational states.

CONCLUSION

In order to try and fully understand and characterize a molecule we have to analyze it in different states of matter. The pulsed beam Fourier transform microwave spectrometer is used to elucidate the gas phase conformation of small molecules and very miniscule intra- and intermolecular interactions such as hydrogen bonding and van der Waals forces. The interactions of the three cases presented in this thesis were detailed using this method. The use of a quantum chemical package like Gaussian 09 [128] is essential in assisting the collection and eventual assignment of the microwave spectra.

The PFBA—FA complex was studied using rotational spectroscopy and high-level *ab initio* calculations. Conformational searches at the B3LYP-D3BJ and MP2 levels of theory identified the same six possible conformers with the lowest energy one being more stable by at least 22 kJ mol^{-1} than the others. This is consistent with the experimental detection of one single conformer. The experimental rotational constants are in excellent agreement with those from B3LYP-D3BJ calculations, indicating that the actual geometry is very similar to the ab initio structure.

The rotational spectrum of TTPA was measured for the first time using both chirped-pulse and cavity-based FTMW spectrometers. Two conformers were observed experimentally and characterized accurately. The rotational spectrum was measured for the tropolone–formic acid doubly hydrogen bonded dimer in the 4.7-9 GHz range using a pulsed-beam Fourier transform

.

microwave spectrometer. It was expected that this doubly hydrogen bonded dimer would exhibit a concerted double proton tunneling motion as the dimer has a C_{2v} symmetry.

For the Tropolone-Formic Acid dimer it would be interesting to analyze the dimer utilizing an energy source that would facilitate the transition state of the dimer. In the hopes of realizing the double proton transfer that was calculated. It would also be of interest to further analyze the out of plane vibrational modes in the hopes of gaining further insight into the system. The analysis of the TTPA-Formic acid dimer is currently being readied for submission for publication.

REFERENCES

[1] D.A. McQuarrie, Quantum Chemistry, 2 edition, University Science Books, Sausalito, Calif, 2007.

[2] D.J.F. M.J. Frisch, G.W. Trucks, H.B. Schlegel, G.E. Scuseria, M. A. Robb, J.R. Cheeseman, G. Scalmani, V. Barone, B. Mennucci, G.A. Petersson, H. Nakatsuji, M. Caricato, X. Li, H.P. Hratchian, A.F. Izmaylov, J. Bloino, G. Zheng, J. L. Sonnenberg, M. Hada, M. Eh, (2010).

[3] H.M. Pickett, J. Mol. Spectrosc. 148 (1991) 371–377.

[4] C.M. Western, B.E. Billinghurst, Phys. Chem. Chem. Phys. Phys. Chem. Chem. Phys 19 (2017) 10222–10226.

[5] C.M. Western, J. Quant. Spectrosc. Radiat. Transf. 186 (2017) 221–242.

[6] US Environmental Protection Agency, Drinking Water Health Advisory for Perfluorooctanoic Acid (PFOA), 2016.

[7] J. Thomas, A. Serrato III, W. Lin, W. Jäger, Y. Xu, Chem. - A Eur. J. 20 (2014) 6148–6153.

[8] D.L. Bryce, R.E. Wasylishen, Acc.Chem.Res. 36 (2003) 327–334.

[9] C.H. Townes, A.L. Schawlow, Microwave Spectroscopy, 2nd editio, Dover Publications, New York, 2012.

[10] Ö. Birer, M. Havenith, Annu. Rev. Phys. Chem. 60 (2009) 263–275.

[11] A.M. Daly, P.R. Bunker, S.G. Kukolich, J. Chem. Phys. 132 (2010) 20–23.

[12] A.M. Daly, P.R. Bunker, S.G. Kukolich, J. Chem. Phys. 133 (2010) 132–133.

[13] A.M. Daly, K.O. Douglass, L.C. Sarkozy, J.L. Neill, M.T. Muckle, D.P. Zaleski, B.H. Pate, S.G. Kukolich, J. Chem. Phys. 135 (2011).

[14] G. Feng, L.B. Favero, A. Maris, A. Vigorito, W. Caminati, R. Meyer, J. Am. Chem. Soc. 134 (2012) 19281–19286.

[15] L. Evangelisti, P. Écija, E.J. Cocinero, F. Castaño, A. Lesarri, W. Caminati, R. Meyer, J. Phys. Chem. Lett. 3 (2012) 3770–3775.

[16] M.C.D. Tayler, B. Ouyang, B.J. Howard, J. Chem. Phys. 134 (2011) 1–10.

[17] A.M. Pejlovas, M. Barfield, S.G. Kukolich, Chem. Phys. Lett. 613 (2014) 86–89.

[18] A.M. Pejlovas, S.G. Kukolich, J. Mol. Spectrosc. 321 (2016) 1–4.

[19] A.M. Pejlovas, W. Lin, S.G. Kukolich, J. Chem. Phys. 143 (2015).

[20] The Editors of Encyclopædia Britannica, (n.d.).

[21] L. Rosenfeld, J.R. Nielsen, eds., in:, Corresp. Princ., Elsevier, 1976, pp. 47–52.

[22] Tipler, Paul, Llewellyn, Ralph, in:, 5th ed., W. H. Freeman and Company., 2008, pp. 160–161.

[23] Lecture Notes, D.G.S. McDonald, University of Salford http://www.cse.salford.ac.uk/physics/gsmcdonald/H-Tutorials/Vector-product-of-vectors.pdf (accessed May 23, 2017).

[24] Rigid Rotor Rotational Energy Levels. Hyperphysics, http://hyperphysics.phy-astr.gsu.edu/hbase/molecule/rotrig.html (accessed March 23, 20172018).

[25] Polar Coordinates Tutorial. Remote Sensing Using Lasers , http://www.seos-project.eu/modules/laser-rs/laser-rs-c03-s01-p01.html (Accessed April 14, 2017).

[26] R. Nave, (2018) 1.

[27] L. de Broglie, Ann. Phys., 10e Série 3 (1925).

[28] C.H. Townes, A.L. Schawlow, Microwave Spectroscopy, Dover, 1975.

[29] P. Atkins, de J. Paula, J. Chem. Inf. Model. 53 (2013) 1689–1699.

[30] P.F. Bernath, Spectra of Atoms and Molecules, 3 edition, Oxford University Press, Oxford ; New York, 2015.

[31] D.A. McQuarrie, Quantum Chemistry, 2 edition, University Science Books, Sausalito, Calif, 2007.Donald A. McQuarrie, Quantum Chemistry, n.d.

[32] Weisstein, Eric W. "Method of Steepest Descent." From *MathWorld*--A Wolfram Web Resource. http://mathworld.wolfram.com/MethodofSteepestDescent.html E.W. Weisstein, MathWorld--A Wolfram Web Resour. (Accessed June 14, 2017.).

[33] S. Grimme, Wiley Interdiscip. Rev. Comput. Mol. Sci. 1 (2011) 211–228.

[34] W. Gordv, Rev. Sci. Instrum. 20 (1948) 668.

[35] C.E. Cleeton, N.H. Williams, Phys. Rev. 45 (1934) 234–237.

[36] J. Ekkers, W.H. Flygare, Rev. Sci. Instrum. 47 (1976) 448–454.

[37] T.J. Balle, W.H. Flygare, Rev. Sci. Instrum. 52 (1981) 33–45.

[38] G.G. Brown, B.C. Dian, K.O. Douglass, S.M. Geyer, S.T. Shipman, B.H. Pate, Rev. Sci. Instrum. 79 (2008).

[39] A. Tang, S. Member, B. Drouin, Y. Kim, G. Virbila, M.F. Chang, L. Fellow, 7 (2017) 244–249.

[40] Y. Xu, J. Van Wijngaarden, W. Jäger, Int. Rev. Phys. Chem. 24 (2005) 301–338.

[41] Encyclopedia of Inorganic Chemistry, 1st ed., Wiley, 2006.

[42] A.M. Pejlovas, A. Serrato, W. Lin, S.G. Kukolich, J. Chem. Phys. 144 (2016) 1–4.

[43] L. Ahrens, J. Environ. Monit. 13 (2011) 20–31.

[44] S. Convention, in:, Propos. to List Pentadecafluorooctanoic Acid (CAS No 335-67-1, PFOA, Perfluorooctanoic Acid), Its Salts PFOA-Related Compd. Annex. A, B and/or C to Stock. Conv. Persistent Org. Pollut., 2009, pp. 1–56.

[45] S.K. Ritter, Environ. Sci. Technol. 88 (2010) 12–17.

[46] G.S. Grubbs II, A. Serrato III, D.A. Obenchain, S.A. Cooke, S.E. Novick, W. Lin, J. Mol. Spectrosc. 275 (2012) 1–4.

[47] G.S. Grubbs, D.A. Obenchain, D.S. Frank, S.E. Novick, S.A. Cooke, A. Serrato, W. Lin, J. Phys. Chem. A 119 (2015) 10475–10480.

[48] M. Losada, H. Tran, Y. Xu, J. Chem. Phys. 128 (2008).

[49] E.B. Bellott E.M. , Wilson, Tetrahedron (1975) 13–15.

[50] R.B. MacKenzie, C.T. Dewberry, K.R. Leopold, J. Phys. Chem. A 118 (2014) 7975–7985.

[51] W.F. Rowe, R.W. Duerst, E.B. Wilson, J. Am. Chem. Soc. 98 (1976) 4021–4023.

[52] S.L. Baughcum, R.W. Duerst, W.F. Rowe, Z. Smith, E.B. Wilson, J. Am. Chem. Soc. 103 (1981) 6296–6303.

[53] S. Baughcum, Z. Smith, E. Wilson, R. Duerst, J. Am. Chem. Soc. 106 (1984) 2260–2265.

[54] P. Turner, S.L. Baughcum, S.L. Coy, Z. Smith, J. Am. Chem. Soc. 106 (1984) 2265–2267.

[55] K. Tanaka, H. Honjo, T. Tanaka, J. Chem. Phys. 110 (1999) 1969.

[56] J.C. Keske, W. Lin, W.C. Pringle, S.E. Novick, T.A. Blake, D.F. Plusquellic, J. Chem. Phys. 124 (2006) 1–13.

[57] L. Evangelisti, G. Feng, Q. Gou, W. Caminati, J. Mol. Spectrosc. 299 (2014) 1–5.

[58] Q. Gou, G. Feng, L. Evangelisti, W. Caminati, Chem. Phys. Lett. 591 (2014) 301–305.

[59] L. Martinache, W. Kresa, M. Wegener, U. Vonmont, A. Bauder, Chem. Phys. 148 (1990) 129–140.

[60] A.M. Pejlovas, W. Lin, S.G. Kukolich, J. Phys. Chem. A 119 (2015) 10016–10021.

[61] J. Thomas, M.J. Carrillo, A. Serrato III, W. Lin, W. Jäger, Y. Xu, Priv. Commun. (2016).

[62] G. Feng, Q. Gou, L. Evangelisti, W. Caminati, Phys. Chem. Chem. Phys. (2013) 2917–2922.

[63] D. Obenchain, S. Cooke, S. Novick, W. Lin, Proc. 71st Int. Symp. Mol. Spectrosc. (2016) 1–1.

[64] W. Jäger, Y. Xu, in:, Handb. High-Resolution Spectrosc., John Wiley & Sons, Ltd, 2011.

[65] Y. Xu, J. Van Wijngaarden, W. Jäger, Int. Rev. Phys. Chem. 24 (2005) 301–338.

[66] R.B. Mackenzie, C.T. Dewberry, K.R. Leopold, Science (80-.). 349 (2015) 58–61.

[67] E.G. Schnitzler, N.A. Seifert, S. Ghosh, J. Thomas, Y. Xu, Phys. Chem. Chem. Phys. 19 (2017) 4440–4446.

[68] M. Becucci, S. Melandri, Chem. Rev. 116 (2016) 5014–5037.

[69] S.P. Dempster, O. Sukhorukov, Q.Y. Lei, W. J??ger, J. Chem. Phys. 137 (2012).

[70] J. Thomas, J. Yiu, J. Rebling, W. Jäger, Y. Xu, J. Phys. Chem. A 117 (2013) 13249–13254.

[71] J.W. Xu Y., J. Chem. Phys. 106 (1997) 7968–7980.

[72] J. Bellet, A. Deldalle, C. Samson, G. Stenbeckeliers, R. Wertheimer, J. Mol. Struct. 9 (1971) 65–75.

[73] PGOPHER version 10.0, C M Western, 2017, University of Bristol Research Data Repository, doi:10.5523/bris.160i6ixoo4kir1jxvawfws047m.

[74] J.K.G. Watson, Vib. Spectra Struct. 6 (1977) 1–89.

[75] J. Thomas, N.A. Seifert, W. Jäger, Y. Xu, Angew. Chemie - Int. Ed. 2 (2017) 6386–6390.

[76] R.F.W. Bader, J. Phys. Chem. A 102 (1998) 7314–7323.

[77] R.F.W. Bader, Chem. Rev. 91 (1991) 893–928.

[78] E.R. Johnson, S. Keinan, P. Mori Sánchez, J. Contreras García, A.J. Cohen, W. Yang, J. Am. Chem. Soc. 132 (2010) 6498–6506.

[79] T. Lu, F. Chen, J. Comput. Chem. 33 (2012) 580–592.

[80] O. Bin, T.G. Starkey, B.J. Howard, J. Phys. Chem. A 111 (2007) 6165–6175.

[81] G.S. Grubbs, D.A. Obenchain, D.S. Frank, S.E. Novick, S.A. Cooke, A. Serrato, W. Lin, J. Phys. Chem. A 119 (2015) 10475–10480.

[82] A.M. Pejlovas, K. Li, S.G. Kukolich, W. Lin, Chem. Phys. Lett. 610–611 (2014) 82–85.

[83] W. Lin, Private Communication .

[84] H. Mollendal, A. Leonov, A. de Meijere, J Phys Chem A Mol Spectrosc Kinet Env. Gen Theory 109 (2005) 6344–6350.

[85] L. Evangelisti, J. Van Wijngaarden, J. Mol. Spectrosc. 290 (2013) 1–4.

[86] J. Thomas, O. Sukhorukov, W. J??ger, Y. Xu, Angew. Chemie - Int. Ed. 52 (2013) 4402–4405.

[87] J. Thomas, F.X. Sunahori, N. Borho, Y. Xu, Chemistry 17 (2011) 4582–4587.

[88] G.G. Brown, B.C. Dian, K.O. Douglass, S.M. Geyer, B.H. Pate, J. Mol. Spectrosc. 238 (2006) 200–212.

[89] G.S. Grubbs, C.T. Dewberry, K.C. Etchison, K.E. Kerr, S.A. Cooke, Rev. Sci. Instrum. 78 (2007) 10–13.

[90] J. Grabow, W. Stahl, H. Dreizler, Rev. Sci. Instrum. 67 (1996) 4072–4084.

[91] C. Møller, M.S. Plesset, Phys. Rev. 46 (1934) 618–622.

[92] A.D. Becke, J. Chem. Phys. 98 (1993) 5648–5652.

[93] R. Krishnan, J.S. Binkley, R. Seeger, J.A. Pople, J. Chem. Phys. 72 (1980) 650–654.

[94] J.K.G. Watson, in:, Handb. High-resolution Spectrosc., 1st ed., American Cancer Society, 2011.

[95] K.B. Wiberg, K.E. Laidig, J. Am. Chem. Soc. 109 (1987) 5935–5943.

[96] A.G. Császár, W.D. Allen, H.F. Schaefer, J. Chem. Phys. 108 (1998) 9751–9764.

[97] Y. Mo, Nat. Chem. 2 (2010) 666–671.

[98] D. Ferro-Costas, N. Otero, A.M. Graña, R.A. Mosquera, J. Comput. Chem. 33 (2012) 2533–2543.

[99] D. Ferro-Costas, R.A. Mosquera, J. Chem. Theory Comput. 9 (2013) 4816–4824.

[100] R.F.W. Bader, Atoms in Molecules: A Quantum Theory, Oxford University Press, Oxford, 1990.

[101] V.M. Stolwijk, B.P. van Eijck, J. Mol. Spectrosc. 113 (1985) 196–207.

[102] B.P. Van Eijck, E. Van Zoeren, J. Mol. Spectrosc. 86 (1984) 75–86.

[103] P. Panini, D. Chopra, in:, Z.-T. Li, L.-Z. Wu (Eds.), Hydrog. Bond. Supramol. Struct., Springer Berlin Heidelberg, Berlin, Heidelberg, 2015, pp. 37–67.

[104] M. Barceló-Oliver, C. Estarellas, A. García-Raso, A. Terrón, A. Frontera, D. Quiñonero, I. Mata, E. Molins, P.M. Deyà, CrystEngComm 12 (2010) 3758.

[105] R.J. Baker, P.E. Colavita, D.M. Murphy, J.A. Platts, J.D. Wallis, J. Phys. Chem. A 116 (2012) 1435–1444.

[106] M. Tsuge, L. Khriachtchev, J. Phys. Chem. A 119 (2015) 2628–2635.

[107] S. Amiri, H.P. Reisenauer, P.R. Schreiner, J. Am. Chem. Soc. 132 (2010) 15902–15904.

[108] P.R. Schreiner, J.P. Wagner, H.P. Reisenauer, D. Gerbig, D. Ley, J. Sarka, A.G. Császár, A. Vaughn, W.D. Allen, J. Am. Chem. Soc. 137 (2015) 7828–7834.

[109] A.E. Bracamonte, P.H. Vaccaro, J. Chem. Phys. 120 (2004) 4638–4657.

[110] L.A. Burns, D. Murdock, P.H. Vaccaro, J. Chem. Phys. 124 (2006) 204307.

[111] D. Murdock, L.A. Burns, P.H. Vaccaro, J. Chem. Phys. 127 (2007) 1–6.

[112] L.A. Burns, D. Murdock, P.H. Vaccaro, J. Chem. Phys. 130 (2009) 144304.

[113] D. Murdock, L.A. Burns, P.H. Vaccaro, Phys. Chem. Chem. Phys. 12 (2010) 8285–8299.

[114] R.L. Redington, T.E. Redington, J. Mol. Spectrosc. 78 (1979) 229–247.

[115] R.L. Redington, T.E. Redington, J. Chem. Phys. 122 (2005) 0–7.

[116] R. Rossetti, L.E. Brus, J. Chem. Phys. 73 (1980) 1546–1550.

[117] Y. Tomioka, M. Ito, N. Mikami, J.Phys.Chem. 87 (1983) 4401–4405.

[118] R.L. Redington, J. Chem. Phys. 113 (2000) 2319–2335.

[119] R.L. Redington, R.L. Sams, J. Phys. Chem. A 106 (2002) 7494–7511.

[120] R.L. Redington, T.E. Redington, R.L. Sams, J. Phys. Chem. A 110 (2006) 9633–9642.

[121] R.L. Redington, T.E. Redington, R.L. Sams, J. Phys. Chem. A 112 (2008) 1480–1492.

[122] H. Sekiya, T. Nakajima, H. Ujita, T. Tsuji, S. Ito, Y. Nishimura, Chem. Phys. Lett. 215 (1993) 499–504.

[123] W. Lin, W.C. Pringle, S.E. Novick, T.A. Blake, J. Phys. Chem. A 113 (2009) 13076–13080.

[124] J. C. Keske, D. F. Plusquellic, (2003).

[125] R.E. Bumgarner, S.G. Kukolich, J. Chem. Phys. 86 (1987) 1083.

[126] B.S. Tackett, C. Karunatilaka, A.M. Daly, S.G. Kukolich, Organometallics 26 (2007) 2070–2076.

[127] Gaussian 09, Revision E.01, M. J. Frisch, G. W. Trucks, H. B. Schlegel, G. E. Scuseria, M. A. Robb, J. R. Cheeseman, G. Scalmani, V. Barone, G. A. Petersson, H. Nakatsuji, X. Li, M. Caricato, A. Marenich, J. Bloino, B. G. Janesko, R. Gomperts, B. Mennucci, H. P. Hratchian, J. V. Ortiz, A. F. Izmaylov, J. L. Sonnenberg, D. Williams-Young, F. Ding, F. Lipparini, F. Egidi, J. Goings, B. Peng, A. Petrone, T. Henderson, D. Ranasinghe, V. G. Zakrzewski, J. Gao, N. Rega, G. Zheng, W. Liang, M. Hada, M. Ehara, K. Toyota, R. Fukuda, J. Hasegawa, M. Ishida, T. Nakajima, Y. Honda, O. Kitao, H. Nakai, T. Vreven, K. Throssell, J. A. Montgomery, Jr., J. E. Peralta, F. Ogliaro, M. Bearpark, J. J. Heyd, E. Brothers, K. N. Kudin, V. N. Staroverov, T. Keith, R. Kobayashi, J. Normand, K. Raghavachari, A. Rendell, J. C. Burant, S. S. Iyengar, J. Tomasi, M. Cossi, J. M. Millam, M. Klene, C. Adamo, R. Cammi, J. W. Ochterski, R. L. Martin, K. Morokuma, O. Farkas, J. B. Foresman, and D. J. Fox, Gaussian, Inc., Wallingford CT,(2013).

[128] T. Oka, J. Mol. Struct. 352–353 (1995) 225–233.

BIOGRAPHICAL SKETCH

Agapito Serrato III, who resides at 1520 West Highway 83 San Benito, Tx. 78586, is currently in his 3rd year of study in the chemistry program at the University of Texas Rio Grande Valley. In May 2018 he graduated with a Master of Science in Chemistry. He graduated from San Benito High School in 1999. While he was attending SBHS, he was concurrently employed at Central Clinic Pharmacy and was employed from June 1995 to February 2012 as a pharmacy technician and recently celebrated his 18th year as a certified pharmacy technician. He had the distinct pleasure of serving others to help facilitate the improvement of their health. In August of 1999 he matriculated at the University of Texas Brownsville and Texas Southmost College and after a period of review he took a leave of absence in 2001. It wasn't until August of 2009 that he resumed his endeavors in higher education. It was during his first semester that he started working under the supervision of Dr. Wei Lin. Since then he has had the pleasure to present his work on various occasions at the Austin Symposium on Molecular Structure and Dynamics in Dallas and at two national American Chemical Society meetings. He has recently also been under the tutelage of Dr. Shervin Fatehi and has immensely enjoyed the rounding out of his previous knowledge and works.